Copyright Warning & Restrictions

The copyright law of the United States (Title 17, United States Code) governs the making of photocopies or other reproductions of copyrighted material.

Under certain conditions specified in the law, libraries and archives are authorized to furnish a photocopy or other reproduction. One of these specified conditions is that the photocopy or reproduction is not to be "used for any purpose other than private study, scholarship, or research." If a, user makes a request for, or later uses, a photocopy or reproduction for purposes in excess of "fair use" that user may be liable for copyright infringement,

This institution reserves the right to refuse to accept a copying order if, in its judgment, fulfillment of the order would involve violation of copyright law.

Please Note: The author retains the copyright while the New Jersey Institute of Technology reserves the right to distribute this thesis or dissertation

Printing note: If you do not wish to print this page, then select "Pages from: first page # to: last page #" on the print dialog screen

NJIT New Jersey's Science & Technology University

The Van Houten library has removed some of the personal information and all signatures from the approval page and biographical sketches of theses and dissertations in order to protect the identity of NJIT graduates and faculty.

ABSTRACT
Improvement of Light Collective Efficiency by Laser-Induced Patterning the Surface of Schottky-Barrier Solar Cells

by
Kejia Fang

In order to achieve maximum light collection efficiency in silicon made solar cells, reflectivity of the silicon surface must be reduced to as low level as possible. In the past, researchers have concentrated on coating the Si surfaces with anti-reflection coatings. Another approach was to form textures on the Si wafers to capture further the light impinging on the solar cells.

Theoretical studies, which were based on ray tracing approach, revealed that some geometrical patterns are better capturing the light than others. In this work, different geometrical surface configurations on a Cu/n-Si Schottky-barrier solar cell have been investigated. The configurations which were considered were V-shaped, M-shaped, asymmetric V-shaped, and asymmetric M-shaped structures. They showed improvement in the short-circuit current over a flat surface solar cells, while the open-circuit voltage remains practically unchanged. Namely, the improvement achieved was not on the expense of the crystallographic structure of the Si surface.

The geometrical surface configurations in a silicon wafer were fabricated by an ultraviolet excimer laser ablation in air, HF, or KOH for similar incident laser power densities and pulse durations. For laser ablation in air,

the Si sample was subsequently processed by annealling and localized etching. The Schottky-barrier solar cell made by laser ablation in air shows slight improvement in light collection efficiency compared to flat surface solar cell. A significant improvement was observed when laser ablation in solutions technique was used.

IMPROVEMENT OF LIGHT COLLECTION EFFICIENCY BY LASER-INDUCED PATTERNING THE SURFACE OF SCHOTTKY-BARRIER SOLAR CELLS

by
Kejia Fang

A Thesis
Submitted to the Faculty of
New Jersey Institute of Technology
in Partial Fulfillment of the Requirement
for the Degree of Master of Science
Department of Electrical and Computer Engineering

May 1992

APPROVAL PAGE

Improvement of Light Collective Efficiency by Laser-induced Patterning the Surface of Schottky-barrier Solar Cells

by
Kejia Fang

May 7, 1992

Dr.Haim Grebel, Thesis Adviser
Associate Professor of Electrical Engineering, Electrical and Computer Engineering, NJIT

5/7/92

Dr. Kenneth Sohn, Committee Member
Assistant Chairperson and Professor of Electrical Engineering, Electrical and Computer Engineering, NJIT

5/7/92

Dr. Nuggehalli M. Ravindra, Committee Member
Associate Professor of Physics, Physics, NJIT

BIOGRAPHICAL SKETCH

Auther: Kejia Fang

Degree: Master of Science in Electrical Engineering

Date: May, 1992

Date of Birth:

Place of Birth:

Undergraduate and Graduate Education:

- Master of Science in Electrical Engineering, New Jersey Institute of Technology, Newark, NJ, 1992
- Bachelor of Science in Electrical Engineering, New Jersey Institute of Technology, Newark, NJ, 1990

Major: Electrical Engineering

ACKNOWLEDGEMENTS

I would like to express my gratitude to my advisor, Dr. Haim Grebel. His mastery of the subject matter combined with a great deal of sincerity and enthusiasm made working on this thesis a good experience.

Many thanks are due to the members of my committee: Dr. Kenneth Sohn and Dr. Nuggehalli M. Ravindra. Their suggestions and discussions have improved the quality of the thesis.

I would also like to thank Prof. Tong for her help in the area of SEM and I-V measurement.

TABLE OF CONTENTS

Page

LIST OF FIGURES

Page

CHAPTER 1

INTRODUCTION

A solar cell is a photovoltaic device designed to convert sunlight into electrical power and to deliver this power into a suitable load in an efficient manner. The most important application for solar cells in the past has been in the space program. The advantages of solar cells lie in their ability to provide nearly permanent, uninterupted power at no operating cost with only heat as a waste product. They also have a high power/weight ratio compared to other power sources. Their chief disavantages lie in the low power/unit area of sunlight, or their relatively low efficiency.

As useful as solar cells have been in the space program, their potential importance for large-scale power generation to meet earth's energy needs is even greater. Today, the rising price of fuel, the realization that limitation of oil and coal supply, and the pollution-free of solar energy, have all led to closer looks at solar energy as an alternative to present day fossil-fuel systems.

A solar cell is a device that converts solar radiation into electrical power. When the solar photons strike on the surface of a semiconductor, they may be reflected, transmitted, or absorbed. The photons that are absorbed by the solar cell are the ones of potential use. When light is absorbed in a semiconductor, it produces two types of free

carriers: the free electron in the conduction band and the free hole in the valence band. Carriers will be generated as long as the solar cell is exposed to light.

Two critical facters, the band gap and the absorption coefficient, determine the absorption of light along with the thickness of the cell. The band gap is the characteristic energy level above which the cell begins to absorb light. Materials which have low band gaps are preferred to take advantage of large fraction of the available sunlight. Different materials absorb sunlight best at different thickness, which can range from about 100 um or more to less than 1 um, [1], [2], [3].

When an n-type semiconductor and a p-type somiconductor are put together in such a way that their fermi levels line up to form a junction, a band bending occurs, creating a potential difference between the p-side and the n-side neutral regions which is called the built-in potential Vbi, shown in Fig. 1.1. This transition region, where the bands bent, is the depletion region, and the dencities of the mobile carriers are equal to zero. Carriers generated from incident photons, under the influence of an electric field, will be accelerated along the electric field within the depletion region in opposite directions (drift current). There is a spatial variation of carrier concentration in the semiconductor then the carriers tend to move from the region of lower concentration, creating the diffusion current. At thermal equilibrium, the net current flow across the

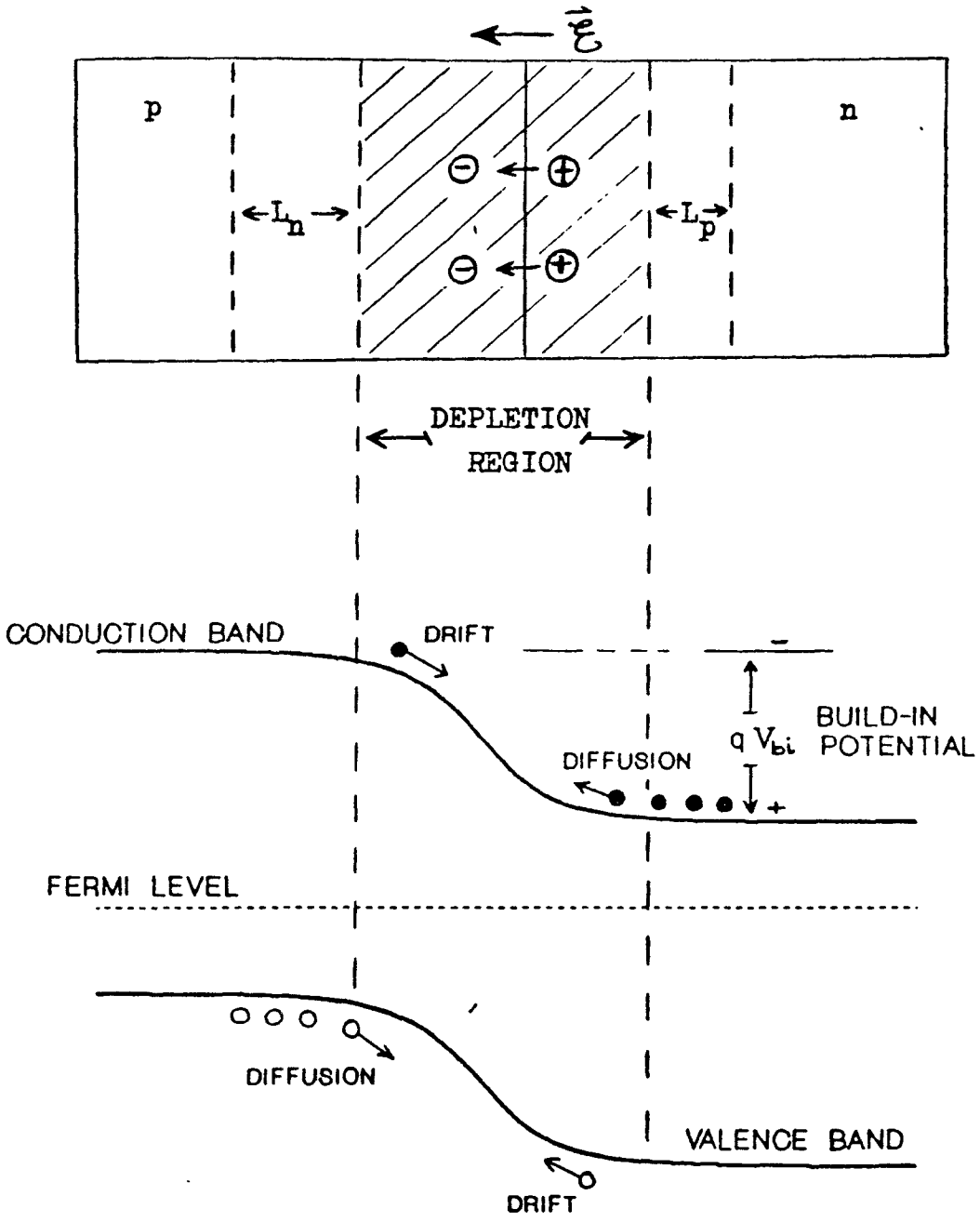

Fig. 1.1 A p-n juction in thermal equilibrium

junction is zero. Thus, for each type of carrier, the drift current due to electric field must equal the diffusion current due to the concentration gradience.

Many of the useful properties of a p-n junction can be achieved by simply forming an appropriate metal-semiconductor contact, or so called Schottky-barrier. Schottky-barrier solar cell has several advantages over regular p-n junction solar cell, which include:

1. Low-temperature processing because no high-temperature diffusion is required.
2. Adaptability to polycrystalline and thin-film solar cells
3. High radiation resistance due to high electric field near the surface.
4. High-current output and good spectral response because of the presence of a depletion region at the semiconductor surface.

The main drawback of Schottky-barrier solar cell is its low open-circuit voltage.

Usually on a Schottky-barrier solar cell, a barrier is created when a low work function metal contacts a p-type semiconductor or a high work function metal contacts a n-type semiconductor. This barrier contact is in contrast to the low-resistance ohmic contact to semiconductor devices. The current transport into metal-semiconductor contact is due mainly to majority carriers, in contrast to p-n junctions, where current transport is due mainly to minority carriers. The band bending in the semiconductor produces a

built-in potential that determines the open-circuit voltage (Voc) in the solar cell. This built-in potential is the difference in work function between the metal and the semiconductor, while the barrier height is the energy difference between the work function of the metal and the bottom of the conduction band of an n-type semiconductor, as shown in Fig. 1.2. The electric field and the band bending within the depletion region are similar to effects for p-n junction.

The metal that contacts semiconductor to create Schottky-barrier is a thin film about 100 A, to optimize for the optical and the electrical properties. The wellknown metals to form Schottky- barrier on n-type silicon are gold and platinum due to their high barrier height on n-type silicon. In our work, copper was used because it is cheap and has acceptable barrier height on n-type silicon. Since our main purpose is to compare the light collection efficiencies of different geometrical surface configurations on Schottky-barrier solar cells, the absolute value of light collection efficiency is not very important.

The reflection of the incident light is of major consideration in the design of solar cells. In order to improve light collection efficiency, we present different geometrical surface configurations on the solar cell surface to increase the number of reflections before light escapes back to space. In our work, five to tweenty percent increase of short-circuit current have been achieved, in comparison

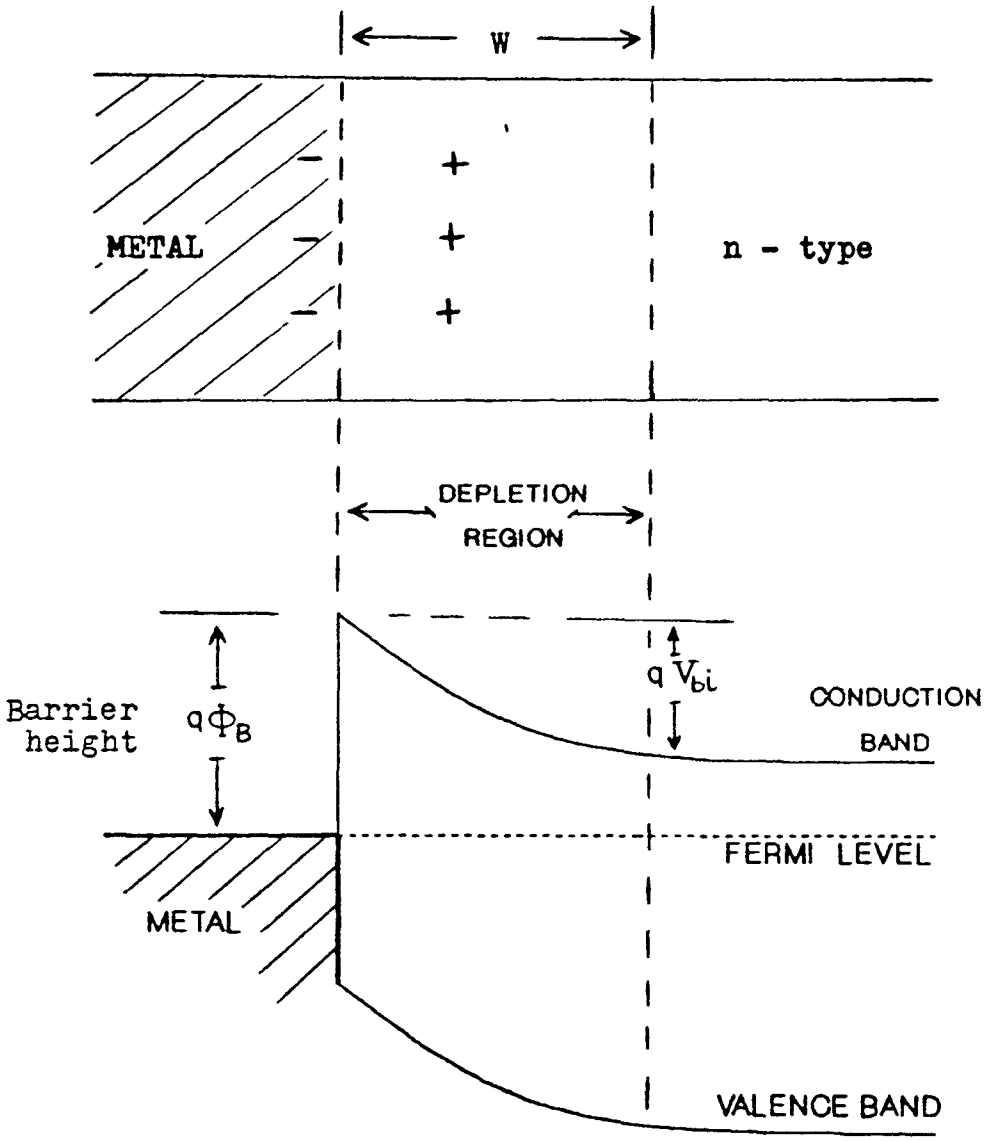

Fig. 1.2 The equilibrium band diagram of a Schottky-barrier of n-type semiconductor

with a flat surface solar cell configuration. These results were achieved without any antireflection coating on either structures.

Researcher in the past, had investigated the formation of randomly distributed regular pyramids on the surface of silicon for space applications which resulted in significant reduction in the overall reflectance of semiconductor surfaces as compared to flat polished surfaces, [6], [7]. This type of textured cells were providing higher short-circuit current mainly due to trapping of light in the bulk of the cell, similally to a green house effect.

V-grooved silicon solar cells were also reported in the mid-70's. These cells showed an improvement of about 20% compared to non-textured cells, mainly because of light reflection reduction from the cell surface, [8]. This reflection reduction was essentially independent of the wavelenth of the incident light. The absorption and carrier generation occured closer to the junction and collection efficiency was thus improved.

In more recent research [9], a substrate with a pyramidally textured top surface and a planer reflecting bottom surface was found to be very successful. It was in point contact solar cells where they proved to demostrate a total efficiencies of 27.5% under concentrated sunlight.

Chemically produced texture surfaces are heavily relying on the crystallographic orientation of the semiconductor materialused. This limits the possibilities of

choosing the optimal patterns. Therefore, we explore other patterning mechanisms to improve the efficiency of Schottky-barrier solar cells.

In order to optimize the solar cell design, we were investigating other geometrical structure to reduce the reflectivity of the cell surface. In our work, four geometrical surface configurations on Schottky-barrier solar cell have been investigated. They were V-shaped, M-shaped, asymmetric V-shaped and asymmetric M-shaped. The experimental results showed improvements of 5% - 20% in short-circuit current over flat cells. The variation of the improvement depents on different configurations and the processing methods.

Conventional way to create geometrical configurations on semiconductor surface is orientation-dependent etching. This method utilizes the fact that some etchants dissolve a given crystal plane of a semiconductor much faster than other planes. A commonly used orientation-dependent etch for silicon consists of a mixture of KOH in water and isopropyl alcohol. The etch rate is 0.6 um/min for the (100)-plane, 0.1 um/min for the (110)-plane, and only 0.006 um/min for the (111)-plane at about 80 C; the ratio of the etch rates for the (100)-, (110)-, and (111)-planes is 100:16:1, [4].

Orientation-dependent etching of (100)-plane oriented silicon creates V grooves with definite shape determined by the crystallographic structures. It is hard to create M-shaped grooves. It is impossible to fabricate asymmetric V-

shaped grooves using orientation-dependent chemical etching. Maskless laser-induced semiconductor processing provides a new way for creating a three dimentional profiles on silicon wafers. The advantages of this technique are:

1. Providing a maskless and photoresistless process to eliminate a contaminating and costly processing stage.
2. Providing a room temperature, non-vacuum process, making it also desirable for compound semiconductors which may be decomposed at relatively high processing temperature.

The approach used in our work is laser ablation in different media, including air, hydrofluoric acid (HF), and potassium hydroxide (KOH).

Laser ablation in air, reffers to rapid thermal melting and/or evaperation of silicon by strong absorption of the UV laser radiation, with little chemistry involved. The prime objective of this approach is that silicon be removed from the appropriate region of the sample as efficiently and cleanly as possible. In fact, the most desirable property of the operation is the ability to localize a surface heat treatment. The aim of the process is to introduce the appropriate amount of energy into the sample in order to melt and evaporate the desired quantity of material to achieve the required structure. Surface patterns are therefore, controlled by the high intensity profile of the laser beam.

In an alternative technique to laser ablation in air, some etching solutions can be added to achieve the same end

result. Since laser ablation in air involves extensive heating and evaporation, sometimes this may have undesirable side-effects on the remainder, such as residual material built-up. The use of chemical reactions can help to reduce the temperature required for removal of material, and simultaneously fine tune the overall material removal process.

The surface configuration profiles are viewed and measured by various ways, including video scanning via optical microscope, scanning electron microscope, and alpha-step measurement.

We found that Schottky-barrier solar cells with surface patterns fabricated by laser ablation in solutions show higher increase in light collection efficiency over flat cells. They also showed improvement over cells with similar surface patterns fabricated in air. The latter patterns, though, have deeper grooves. It suggests that the improvement in light collection coefficiency in solar cells due to the surface patterns, may have partially offseted by crystal structure degradation in the small area exposed to high temperatures in air. Laser ablation in solutions is almost a damage-free processing presumably because of the smaller temperatures involved, and the incorporation of a low thermal processing such as photo-electrochemical reaction.

CHAPTER 2

THEORY and ANALYSIS

2.1 Laser Ablation in Air

The field of laser-induced processes is inherently multidisciplinary. Upon impact of a laser beam on silicon, electromagnetic energy is converted first into electronic excitation and then into thermal, chemical and mechanical energy. In the whole process the molecular structure as well as the shape of the material are changed in various ways.

2.1.1 Absorption of Laser Light

In order to cause any lasting effect on a material, laser must first be absorbed. Absorption is the most critical step in laser processing. The optical properties of the solid can be described in terms of macroscope optical constants, the refractive index n, and the extinction coefficient k with $k = \alpha \lambda / 4\pi$, where is the absorption coefficient of the material at the wavelength. The intensity reflection coefficient R at normal incident is given by

$$R = \frac{(n-1)^2 + k^2}{(n+1)^2 + k^2} \qquad (2.1)$$

The reflection and the absorption coefficients determine the amount of beam power absorbed within the material.

Fig. 2.1, 2.2 show the absorption and reflection coefficients as a function of wavelength for crystalline Si (Eg=1.1eV, corresponding to λ = 1.13 um), and quartz

(Eg=6.9eV, corresponding to a wavelength of 180 nm, which also plays an important role in our experiment). Both materials exhibit the same essential feartures: absorption peaks around 10 um due to phonon coupling, weak absorption at intermediate wavelengths and a steep increase in absorption as the photon energy approches the band gap.

With reference to Fig. 2.1, it is noted that the absorption coefficient of Si increases with decreasing laser wavelength only gradually near 1.13 um ($\hbar w$ = 1.1 eV), but rather abruptly near 0.36 um ($\hbar w$ = 3.4 eV). The explanation is that there are two different kinds of interband transitions in silicon as shown in Fig. 2.3. The first kind, direct transitions, lead from valence-band to conduction-band states with the same wave vector. Such transitions are possible in Si only at photon energies excessing its direct gap at 3.4 eV. The second kind of interband transitions, indirect transitions, involve valence- and conduction-band states of different wave vector. Since the fundamental gap at 1.1eV is an indirect gap, it allows only phonon-assisted transitions. The probability of such transitions depends on the phonon occupancy and is relatively small and temperature dependent [11]. In order to achieve high absorption coefficient in silicon, laser with short wavelength should be utilized.

2.1.2 Laser-Induced Heating

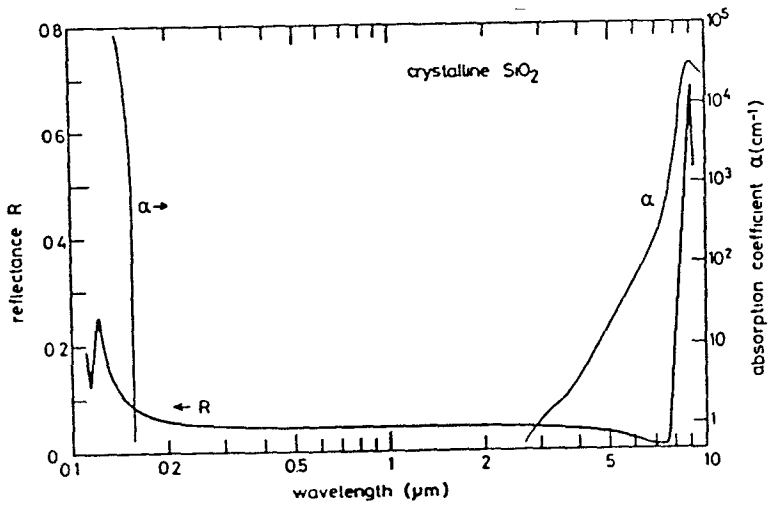

Fig. 2.1 Reflectance and absorption coefficient as a function of wavelength for crystalline quartz (ref.[11])

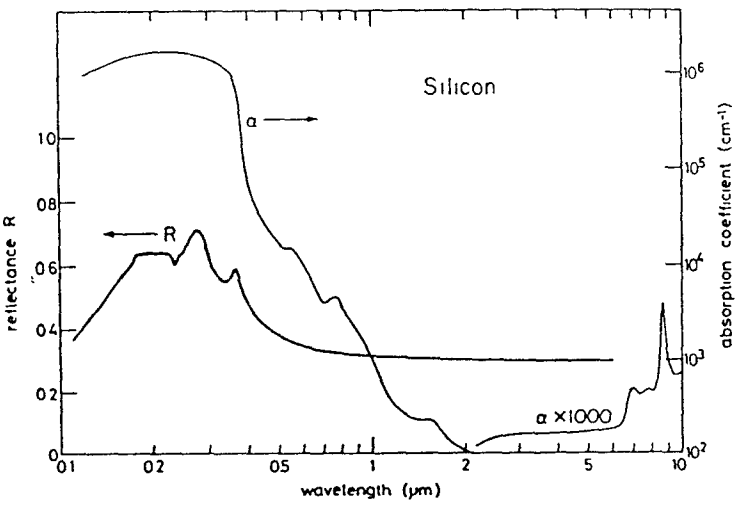

Fig. 2.2 Reflectance and absorption coefficient as a function of wavelength for crystalline silicon (ref.[11])

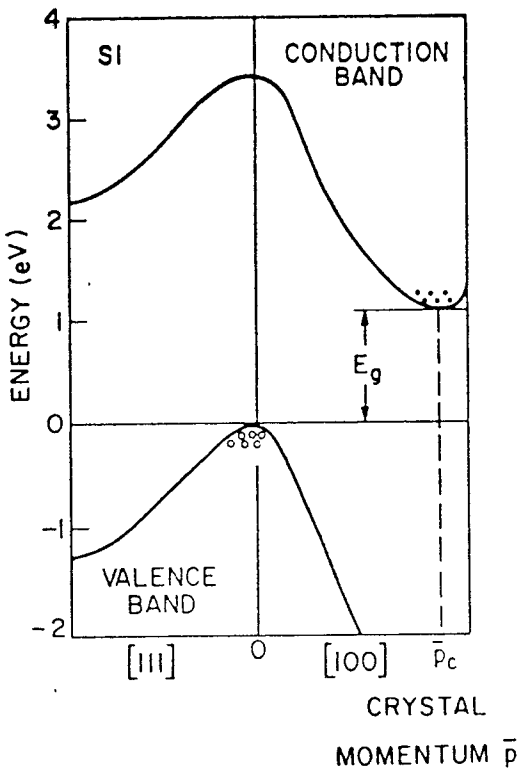

Fig. 2.3 Energy band structure of Si (ref.[4])

The absorbed energy increases the density of free electrons and holes, and also provides them with a significant amount of kinetic and potential energy. Once energy has been coupled into the carrier system, it must be redistributed amongst the other carriers. Ultimately, the material may heat ut significantly in an extremely short time.

The energy exchanges occur by several mechanisms within the electronic system itself. The various electron scattering times in silicon are plotted in Fig. 2.4. As shown in the figure, the scattering processes are extremely rapid, accurring in time of the order of 10 fs for densities around 10 carriers per cm . Energy may escape from this system via carrier-phonon scattering, and in this way the lattice will heat up according to the number of lattice phonons created. The lattice is heated almost instantaneously as a consequence of direct irradiation by intense laser beams.

Fig. 2.5 shows the temperature rise induced in silicon as a function of the ratio of absorbed argon laser beam power over the beam radius, for a range of pre-chosen substrate temperatures. If the temperature reaches melting point or even higher, melting or evaporation occurs near the boiling temperature of silicon, part of the energy that is incident on the sample surface will be scattering away from it by the evaporation.

Because of the large nonlinearities associated with laser heat of silicon, it is very difficult to estimate the

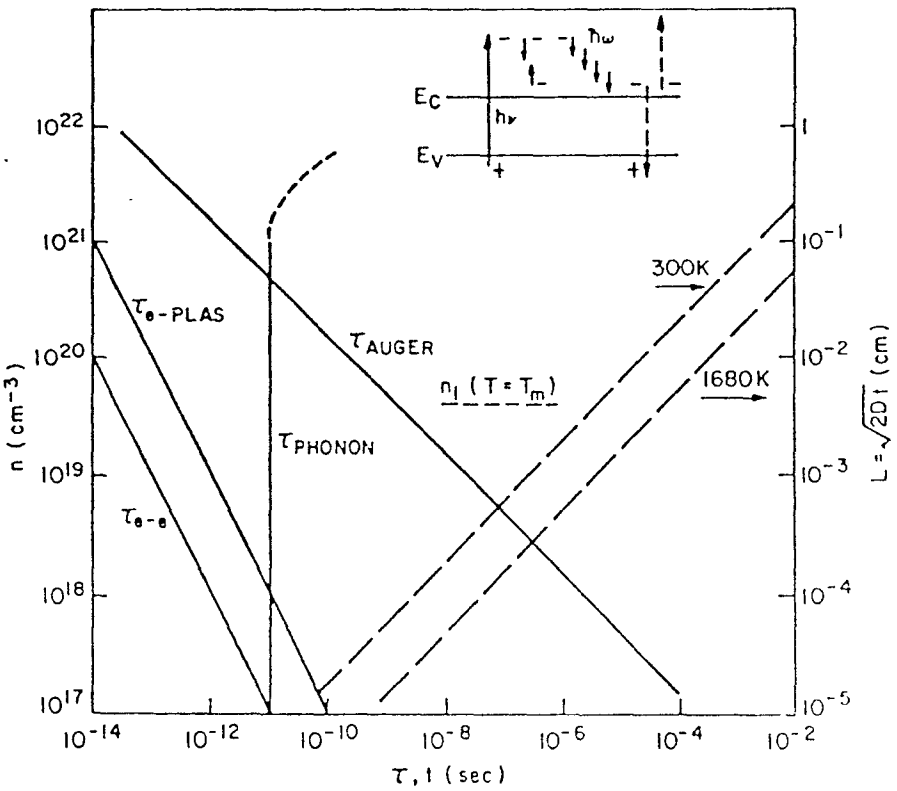

Fig. 2.4 The various electron scattering times in silicon. Also included are the characteristic heat diffusion lengths for silicon at two temperatures in the solid phase. The insert is a schematic of some of the important scattering processes. The vertical axes show the carrier density, and the thermal diffusion length (ref.[12])

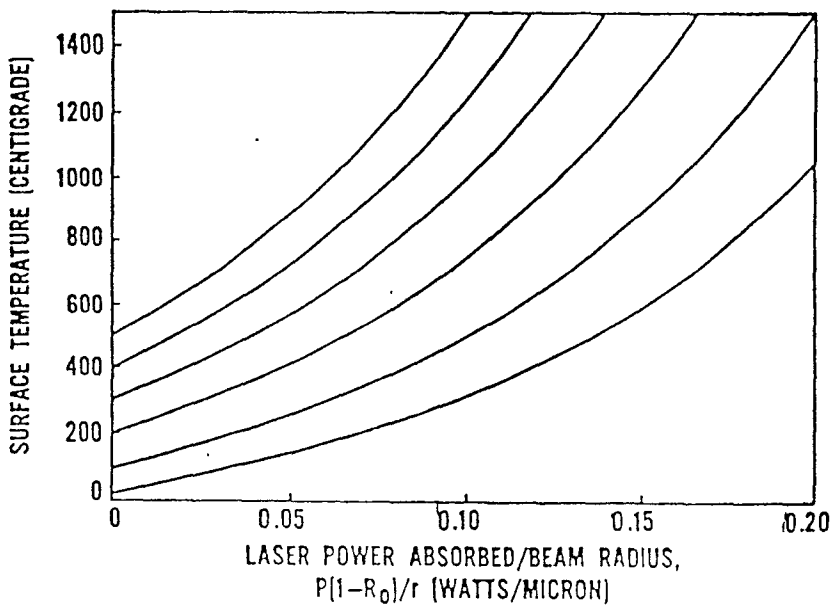

Fig. 2.5 Temperature rise induced in silicon as a function of the ration of absorbed argon laser beam power over the beam radius (ref.[14])

power required to achieve a required processing temperature. Nevertheless, it is not difficult to determine if melting or evaporation occurs by the experiment. Thus, the power of incident laser beam can be determined. By using short-pulsed, highly focused laser beam, the appropriate amount of energy may be introduced into the sample to melt and evaporate the desired quantity of material in order to achieve the required structure, without unnecessarily heating up the remainder of the sample. That is the aim of laser ablation in air.

Although high temperature during the laser ablation in air may cause localized crystalline damage, its highly effective removal ability makes it acceptable approch to fabricate surface configurations. In order to compensate for the drawback of this approach, that is, material residue around the melted points, the samples are annealed in well vacuumed environment in order to recover silicon's initial high degree of crystallinity, followed by localized chemical etching to remove the remaining degraded material.

2.2 Laser Ablation in Solutions

Optical excitation of a semiconductor/electrolyte system may lead to enhanced or induced chemical reactions. In general, the incident photon energy can be deposited in the etching medium and/or the semiconductor sample. A fraction of the absorbed photon energy has to be transformed into the chemical energy that is used in the chemical reactions. When

incident light is absorbed primarily in the semiconductor, two different effects may occur. First, absorbed optical energy can be transformed into heat. The resulting temperature rise in the material can increase a thermally activated reaction rate or other thermal processes. Second, photo-generated carriers may participate directly in etching reactions at the solid surface.

2.2.1 Effect of Illumination on Charge Transfer Across Semiconductor/Solution Interface

Since the semiconductor specimen is in contact with the electrolyte, and they have different Fermi levels, we may assume that the contact is a Schottky-barrier [4]. The band diagram for the ideal semiconductor/solution contact is shown in Fig. 2.6. Fig. 2.6a shows the energy band diagram of an isolated electrolyte adjacent to an isolated n-type semiconductor. The analogous form of E_f in an electrolyte is provided by the energy level E_{redox} [29]. When two materials make intimate contact, two Fermi levels must be equal at thermal equilibrium and the vacuum level must be continuous so that the band diagram will become as shown in Fig. 2.6b.

When an n-type semiconductor/solution interface is illuminated by a laser with a photon energy greater than the bandgap energy, electrons and holes are created in the solid. Photo-generated holes drift to the interface under the influence of the space-charge field in the depletion

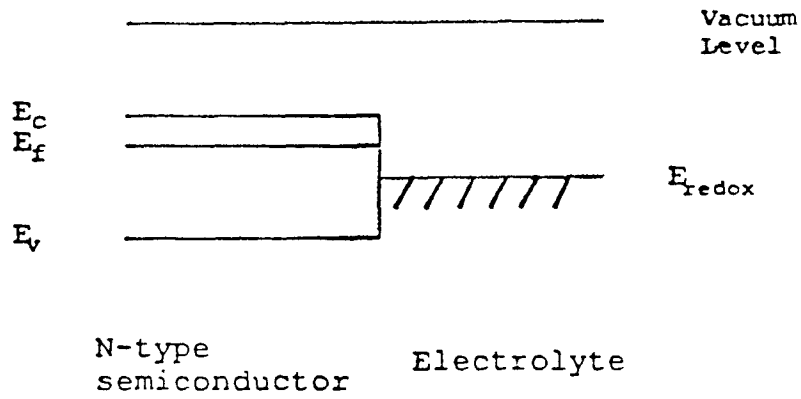

(a)

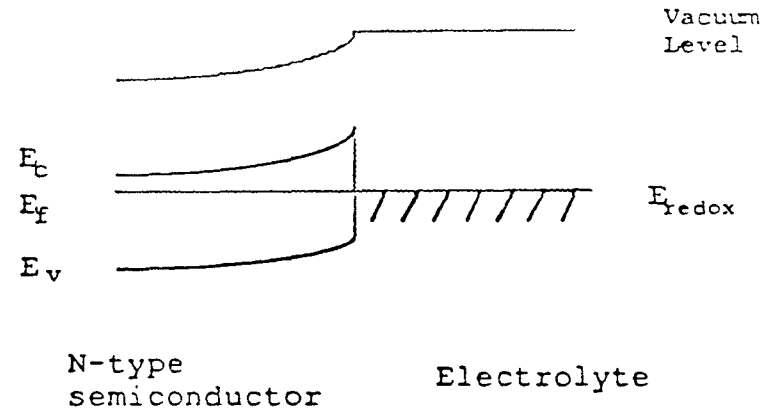

(b)

Fig. 2.6 (a) Energy band diagram of an isolated electrolyte adjacent to n-type semiconductor under nonequilibrium. (b) Energy band diagram of a electrolyte/semiconductor conatct in thermal equilibrium.

region where they induce an oxidative decomposition reaction [30]. Fig. 2.7 shows the band diagram of this case.

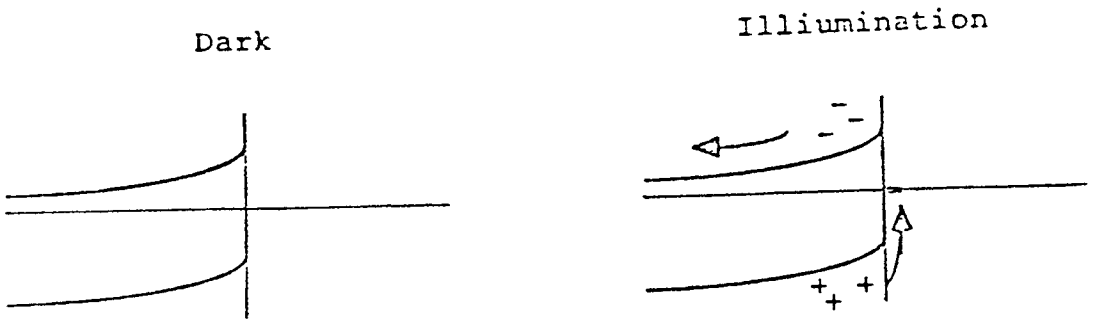

Fig. 2.7 (a) The band diagram of electrolyte/semiconductor surface. (b) The energy band under illumination.

The reactions underlying semiconductor etching processing are electrochemical, and are accompanied by the transfer of electrical charge across the semiconductor/solution interface [31]. In our case, silicon is converted to a higher oxidation state by the reaction:

$$Si + 2h^{+} \text{---} Si^{2+} \qquad (2.2)$$

The oxidation reaction requires 2 holes for its reaction. The primary oxidizing species in semiconductor etching is OH , which is formed by the dissociation of water:

$$H_2O \rightleftharpoons OH^{-} + H^{+} \qquad (2.3)$$

The Si^{2+} in Eq.(2.2) combines with OH^{-} to give

$$Si^{2+} + 2OH^{-} \longrightarrow Si(OH)_2 \qquad (2.4)$$

which subsequently releases hydrogen to form SiO

$$Si(OH)_2 \longrightarrow SiO_2 + H_2 \qquad (2.5)$$

Hydrofluoric acid (HF) is used to dissolve SiO. The reaction is

$$SiO_2 + 6HF \longrightarrow H_2SiF_6 + H_2O \qquad (2.6)$$

where H_2SiF_6 is soluble in water.

2.2.2 Heating Effect in Laser-Induced Chemical Reaction

An important approach to accelerate laser-induced chemical etching used laser heating of the semiconductor surface. A scheme for the etching of semiconductors made use of simultaneous localized melting and etching [15]. In this scheme, a focused argon-ion laser, with intensities of the order of 10^6 to 10^7 W/cm^2, was used to fabricate slots, blind holes, and through-holes in silicon immersed in KOH solution.

For the material removal process, it is possible that the melting and/or evaporation contribute to direct removal of material. Without melting or evaporation, the etch or total material removal rate would be much smaller. The instantaneous removal rates may vary with pulse duration and degree of focusing that can be achieved, i.e., incident power density.

2.3 Schottky-Barrier Solar Cells

When a metal is brought into contact with a clean surface of semiconductor material, a readjustment of charge takes place in order to establish thermal equilibrium and an energy band bending occurs at the interface. If the metal is thin enough

to be partially transpatent to light, then some of the incident light can penetrate to the semiconductor and a photocurrent will result. Fig. 2.8 shows the most simple form of an n-type Schottky-barrier device and defines some

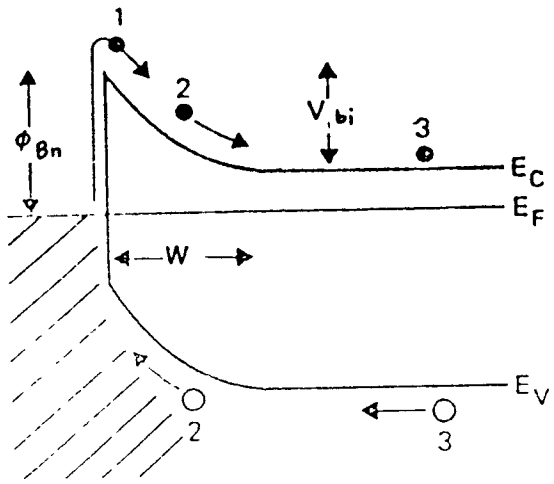

Fig. 2.8 Energy bang diagram of a Schottky-barrier on an n-type semiconductor.

of its important parameters, the depletion width W, the barrier height ϕ_{Bn} and the built-inpotential V_{bi}. There are three photoeffects that can take place. Light can be absorbed in the metal and excite electrons over the barrier into the semiconductor (1 in Fig. 2.8), shorter wavelength light entering the semiconductor is mostly absorbed in the depletion region (2 in Fig. 2.8), while longer wavelength light is usually absorbed deep in the semiconductor (3 in Fig. 2.8).

The excitation of carriers from the metal into the semiconductor is much smaller than the band-to-band excitation mechnisms (2 and 3 in Fig. 2.8), and can be neglected compared to the others. Therefore, as far as the photocurrent generation and collection are concerned, the Schottky-barrier solar cell can be treated as a p-n junction with a zero juction depth but with an attenuating metal coating at its surface. The high field in the depletion region of the Schottky cell serves the same function as the drift field in the diffused region of a normal p-n cell in overcoming surface loses.

2.3.1 Photocurrent in Schottky-Barrier Solar Cells

The two major contributions to the spectralresponse and to the phtocurrent come from the depletion region and from the bulk. Since the high field in the depletion region sweeps carriers out before they can recombine, leading to a current for a monochromatic light equal to

$$J_d = qT(\lambda)F(\lambda)[1-\exp(-\alpha W)] \qquad (2.7)$$

where $T(\lambda)$ is the tranmission coefficient at the metal/ semiconductor interface, $F(\lambda)$ is the incident photon flux, a is the absorption coefficient, and W is the width of the depletion region.

The collection from the base of the Schottky-barrier cell is qualitatively the same as from the base of a p-n junction cell. If the back contact is ohmic, and the device thickness is much greater than the diffusion length, the

photocurrent due to holes collected from the n-type base region is then simplified to

$$J_p = T[qF\alpha L_p/(\alpha L_p + 1)]\exp(-\alpha W) \qquad (2.8)$$

The total photocurrent is found by adding (2.7) to (2.8). This photocurrent may be reduced if there is an interfacial layer such as an oxide or another insulator more than 30 Å thick between the metal and the semiconductor. For thinner oxide layers than this, tunneling can take place and the photocurrent will not be seriously affected by the oxide layer.

The equivalent circuit for a Schottky-barrier solar cell is shown in Fig. 2.9, where a constant-current source is in parallel with the metal/semiconductor interface. The source I_L results from the excitation, I_S is the diode saturation current, and R_L is the load resistance.

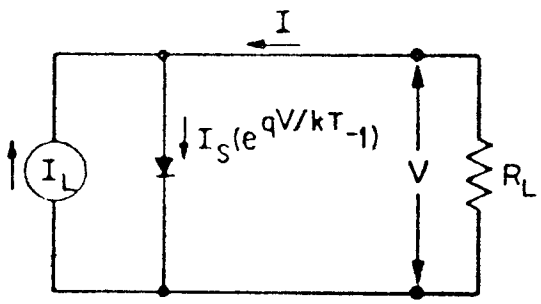

Fig. 2.9 Idealized equivalent circuit of a solar cell

The ideal I-V characteristics of the Schottky-barrier solar cell are given by

$$I = Is[\exp(qV/KT) - 1] - I_L \qquad (2.9)$$

and

$$J_S = I_S/A = A^{**} T \exp(-q\phi_{Bn}/KT) \qquad (2.10)$$

where A^{**} is the effective Richardson constant (for n-type Si is 110 A/cm^2-K^2).

From Eq. (2.10), we can see that the saturation current depends very much on Schottky-barrier height, and fundamentally different from the forward bias saturation current in p-n junction.

2.3.2 The Surface Configurations of Schottky-Barrier Solar Cells

In this thesis, four surface configurations have been investigated. They are V-shaped, asymmetric V-shaped, M-shaped, asymmetric M-shaped surface configurations. From reflection point of view, flat surface Schottky-barrier solar cell experiences only one reflection (or transmission), while the solar cells with patterned surface can experiences more than one reflection (or transmission), as shown in Fig. 2.10 - 2.13. From these figures, we can see that light is reflected by a grooved surface more than once before it escapes back to space.

2.3.3 Barrier Height and Ohmic Contact

Barrier height is an important parameter in metal/semiconductor devices. As discussed in section 2.3.1, the saturation current depends on barrier height. For moderately

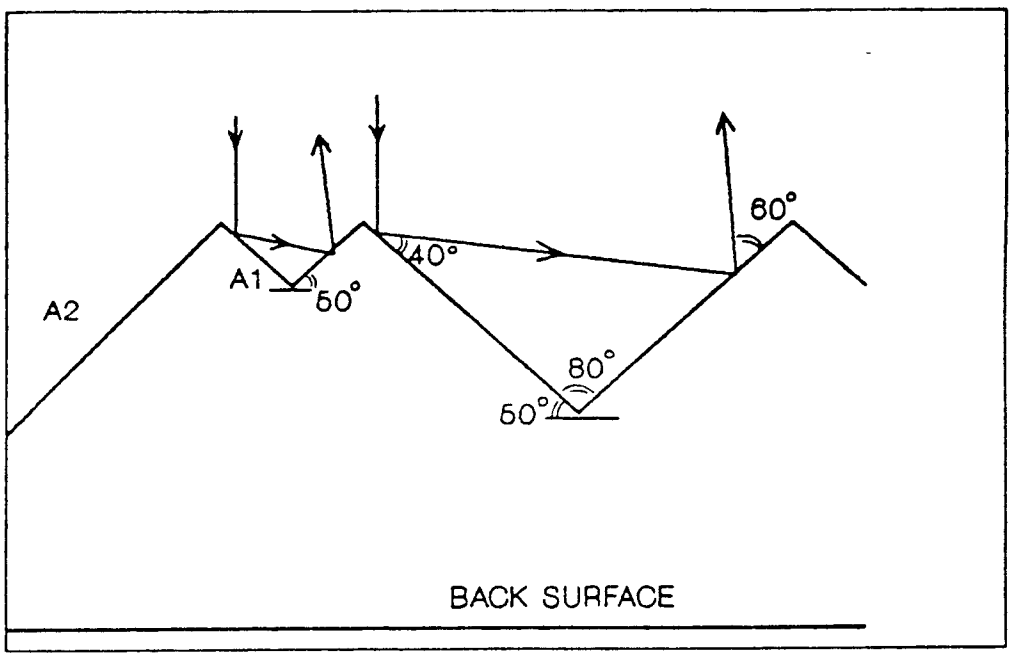

Fig. 2.10 The M-shaped surface cell

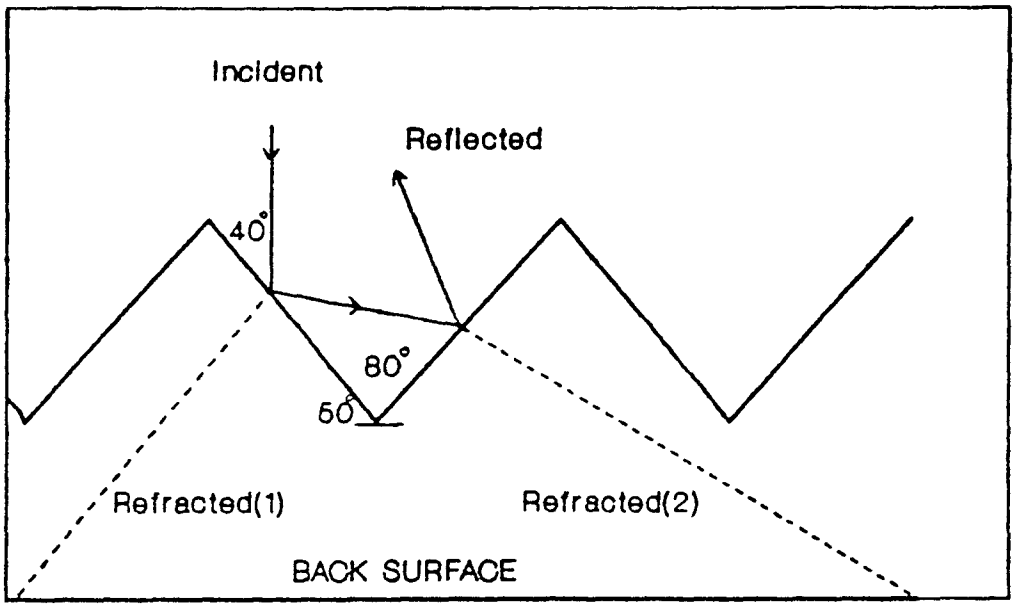

Fig. 2.11 The V-shaped surface cell (50°)

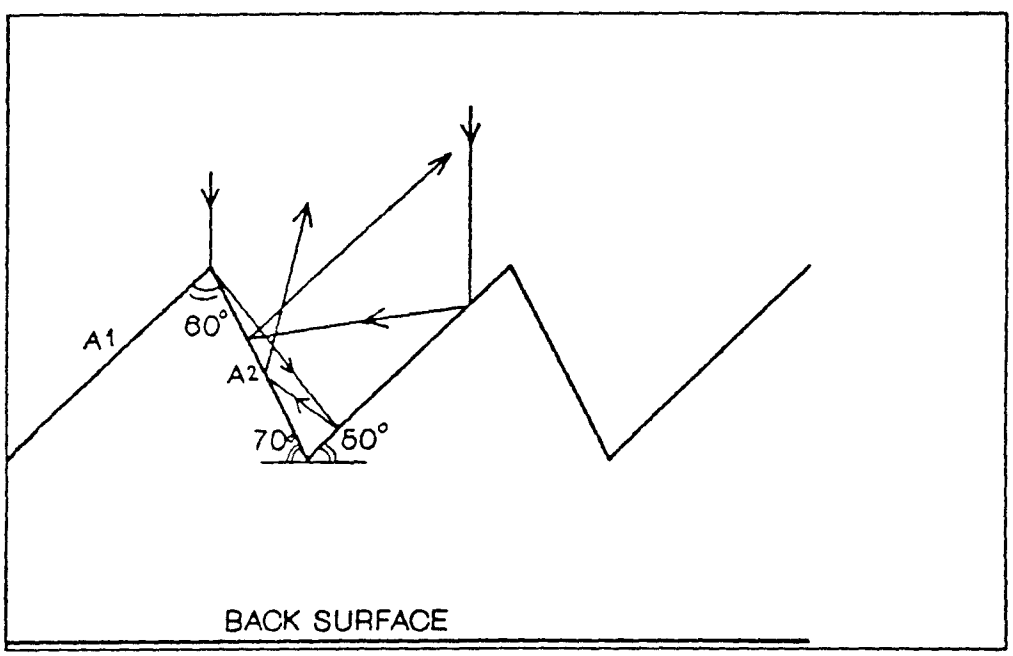

Fig. 2.12 The Asymmetric-V-shaped surface

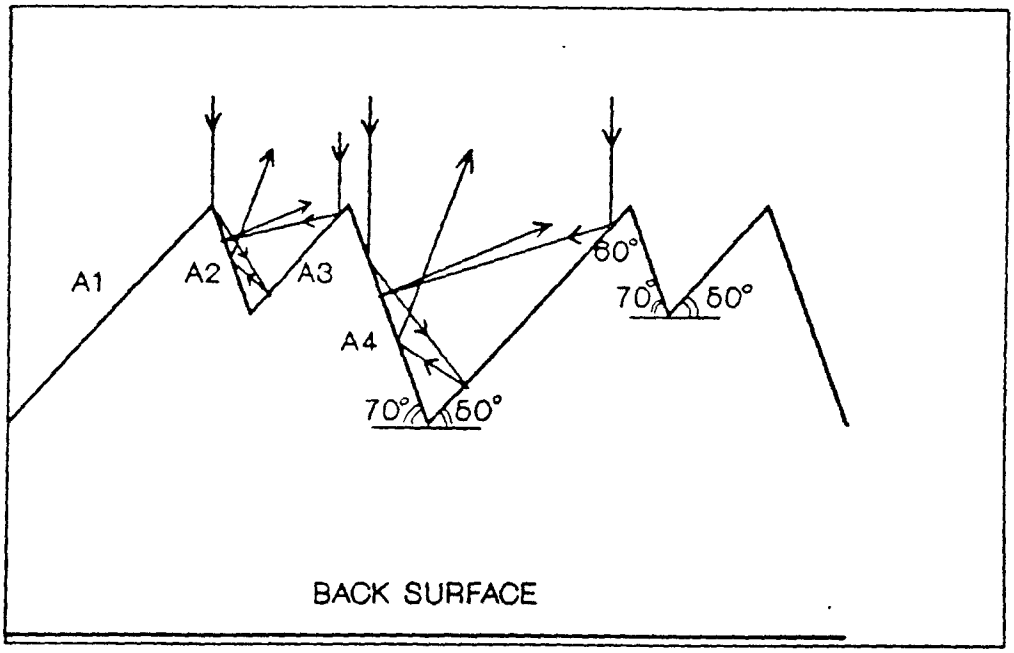

Fig. 2.13 An Asymmetric-M-shaped surface

doped semiconductors, the I-V characteristics in the forward direction is given by

$$I = Is[\exp(qV/KT) - 1] \tag{2.11}$$

where

$$I_S = AA^{**}T \exp(-q\phi_B/KT) \tag{2.12}$$

From Eq. (2.11), the barrier height can be calculated from the current I , which is determined by an extrapolation of the log (I) versus V curve to V = 0. The barrier height is calculated from I in Eq. (2-12) according to

$$\phi_B = (KT/q)\ln(AA^{**}T^2/Is) \tag{2.13}$$

An ohmic contact is defined as a metal/semiconductor contact that has s very small contact resistance of the semiconductor. A good ohmic contact should not significantly degrade device performance, and it can pass the required current with a voltage drop that is sufficiently small compared with the drop across the active region of the device.

The specific contact resistance for ohmic contact is defined as [4]

$$R_c = \left[\frac{\partial J}{\partial V}\right]^{-1}_{v=0} \quad \Omega\text{-cm} \tag{2.14}$$

For metal/semiconductor contacts with low doping concentrations, the thermaionic emission current dominates the current transport. Therefore,

$$R_c = (K/qA^*T)\exp(q\phi_{Bn}/KT) \tag{2.15}$$

From Eq. (2.15), we can see that low barrier height material should be used in order to get a small Rc. A schemetic of

thermionic emission over the low barrier is shown in Fig. 2.14.

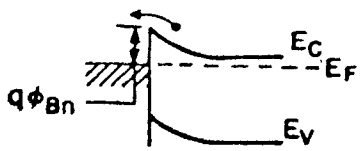

Fig. 2-14 Schemetic of thermionic emission over the low barrier.

CHAPTER 3

EXPERIMENTS

3.1 System Setup for Laser-Induced Interaction with Silicon

3.1.1 System Setup

The main components of our experimental setup for laser-induced etching consist of a laser, a set of optic system, and a translation stage. For laser-induced chemical etching, a reaction environment must be created. The laser light can be incident perpendicular or tilted with respect to the surface of the substrate. The laser beam is scanned over the substrate or focused to a line by means of a cylindrical lens (Fig. 3.1). The whole system setup is shown in Fig. 3.2.

3.1.2 Laser

The laser that is used in our experiment is KrF excimer laser with wavelength of 248 nm, pulse duration of about 10 ns, and average output power of 30 W. The main advantage of this laser is its high photon energy as discussed in section 2.2. Such a high power pulsed laser is an ideal source for our laser-induced etching in air where rapid heating and cooling rates and good energy localization within a thin surface layer are required. On the other hand, since we mainly focus on large area processing, high power laser is desirable. In this case, processing times can be significantly reduced by large-area focus in a large volume

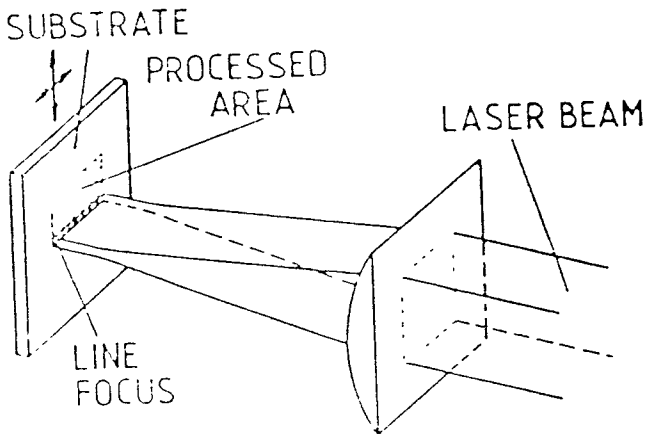

Fig. 3.1 Schematic showing the focusing in large-area chemical processing in perpendicular configuration (ref.[15])

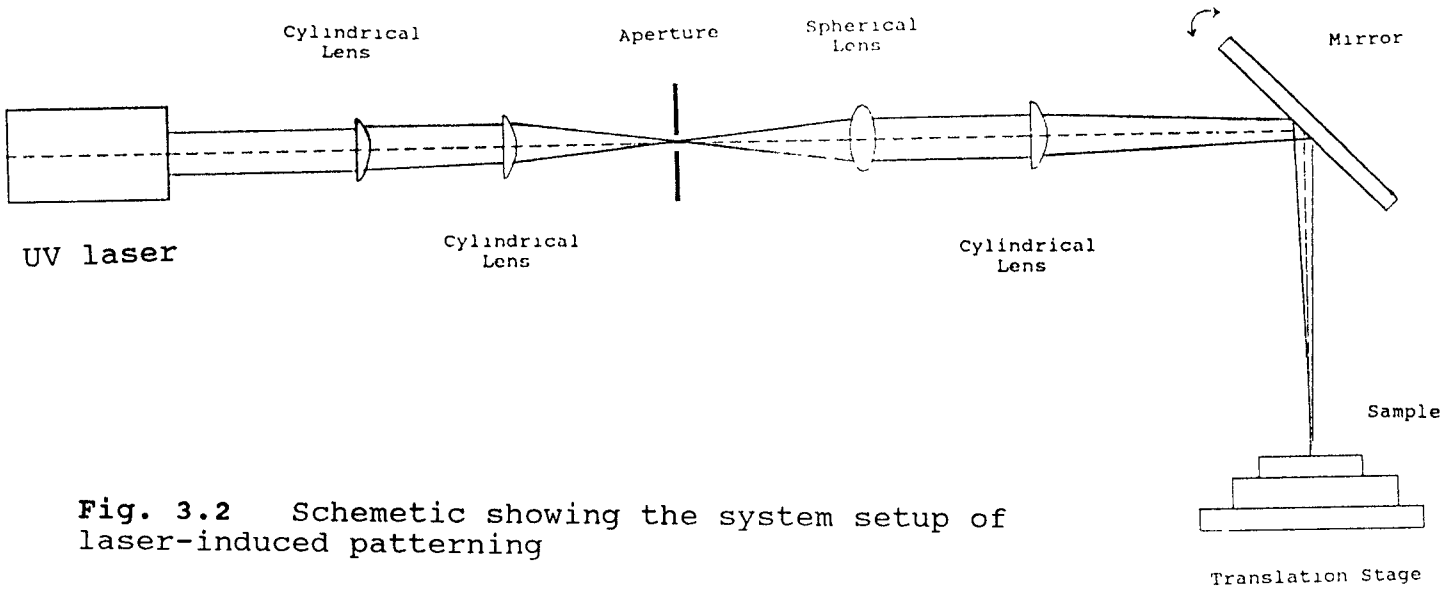

Fig. 3.2 Schemetic showing the system setup of laser-induced patterning

above the substrate surface

High power pulse laser has its disavantages though: Damaging of the substrate surface structure, and non-uniformity and morphology of generated patterns due to uncontrolled surface melting or evaporation. It is also rather difficult to focus the excimer laser beam due to its relatively poor coherence (an excimer laser's output is highly multimode and contains as many as 10^5 transverse modes).

In order to overcome these drawbacks, some techniques have been used, including: anealling and localised etching after laser etching to recover the initial high grade crystallinity and removal of damaged structures; placing an aperture in the focal plane of two cylindrical lens (see Fig. 3.2) to eliminate high order modes, and improve the quality of the laser beam.

3.2 Material Preparation

3.2.1 Surface Treatment

Single crystal wafers of n-type silicon were used in the expariments. The dopant contrentration was approximately 10^{16} /cm^3 . All wafers had a (100) crystal orientation parallel to the surface. Both surfaces of the wafers were mirror-polished by a chemo-mechanical method, so that no further mechanical polishing was required.

The contaminations on the specimen surface should be removed prior to the laser process, since they may interfere

with the etching by undesirable reactions with the etchant or degrade the surface structure during the laser direct writing process. In our experiments, the following steps were used to give a flat and damage-free surface:

1. Polish in Bromine-methanol (Br :CH OH = 1:99 by vol.%) for 1 min.
2. Rinse with methanol for 30 sec.
3. Wash in distilled, deionized water for 30 sec.
4. Etch in dilute Hydrofluoric acid (HF(48%):H O = 1:9 by vol.%) for 30 sec.
5. Wash in deionized water for 30 sec.
6. Air blow-dry immediately.

3.2.2 Electrolyte

Two well-known electrolyte were used. One etchant was a mixture of HF:H O with a ratio of 1:20 by volume, the other was orientation-dependent etchant, KOH:H O, with a ratio of 1:20 by weight. Both aqueous solutions were of sufficient dilution that little or no dark etching were present.

3.3 Laser Ablation

3.3.1 Laser Ablation in Air

The groove configurations were formed by focusing a laser beam on silicon surface. In order to get high resolution grooved patterns, the laser beam was focused on the surface of the substrate by carefuly adjusting its position. The scheme of the arrangement used to produce the pattern is

shown in Fig. 3.2. Periodic structures have been created by moving the substrate in perpendicular direction to the etched line, one step at a time. By tilting the reflection mirror (see Fig. 3.2), we can change the incident angle of the laser beam to fabricate asymetric grooves.

After the laser ablation, the samples were placed in a vacuum chamber, where they were anealled at temperature of 600 C for 30 min., then cooled down to room temperature. After anealling, the samples were put into 10 wt.% KOH solution for 5 min. in order to remove the degraded material.

3.3.2 Thin-Film Cell Configuration

After the silicon specimen had been cleaned as described in section 3.2.1, a small quantity of the electrolyte solution was dropped on the specimen surface by a neutralization pipet. Then a quartz was put on the specimen. An electrolyte thickness of about 50 um was held by capillary action between the silicon substrate and the cover quartz. Quartz was used as cover due to its low absorption coefficient in the wavelength of the ablating laser. The silicon substrate was then processed under the illumination of the focused laser beam. The cell configuration is shown in Fig. 3.3.

Repeated procedure, as discussed in section 3.3.1, created various surface configurations in solutions (5 wt.% KOH or 5 vol.% HF).

3.4 Measurement of Groove Profile

Four methods were used to measure the profile of the surface patterns. These are: diffraction modes measurement, video scanning system, scanning electron microscope, and alpha-step recorder measurement.

In the early stage of our experiments, we measured the diffraction modes intensity to calculate the groove configurations by Fourier Analysis. Since the method is indirect and inaccurate, it was soon replaced by other methods.

In the video scanning system the image of the grooves' profile is viewed by a video camera through a microscope. The dimensions of the profile were then recorded from the video imager. Fig. 3.4 shows the schematic arrangement.

A schematic representation of a scanning electron microscope is shown in Fig. 3.5. The SEM has inherently higher resolution than optical system. The image in an SEM is produced by scanning the sample with a focused electron beam and detecting the secondary electrons, and the image is displayed on a CRT scanned in synchronism with the sample beam scan in the SEM.

The alpha-step instrument measures the groove profile by using a very thin needle across the grooves and recording the movement of the needle in perpendicular direction to the sample surface grooves.

3.5 Metal-Semiconductor Contact Preparation

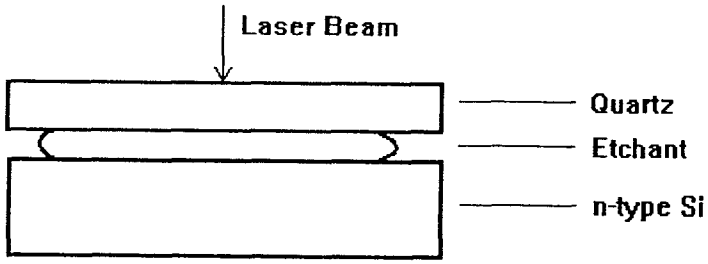

Fig. 3.3 The thin-film cell configuration

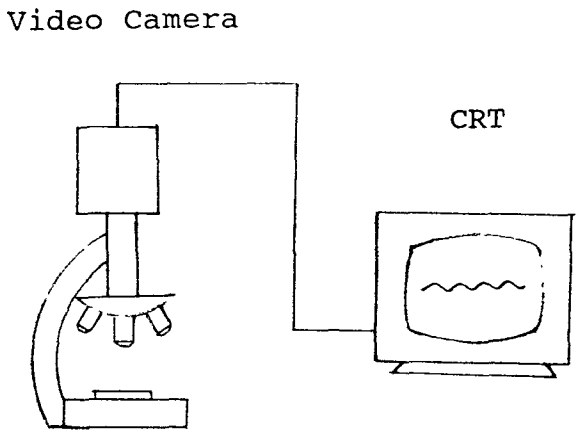

Fig. 3.4 Schematic of video scanning system

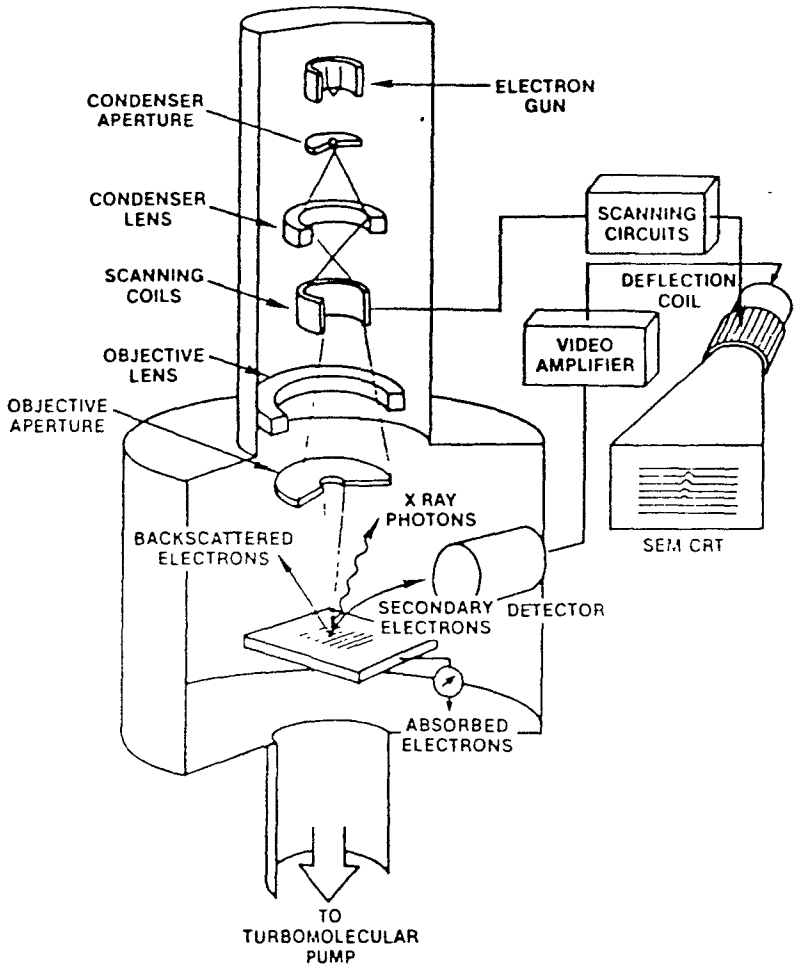

Fig. 3.5 A schematic representation of a scanning electron microscope

3.5.1 Material Preparation and Surface Treatment

Copper was deposited on silicon surface to form a Schottky-barrier contact. Aluminum was deposite on the back side of the substrate to form the ohmic contact. Both are highly purified materials.

The silicon wafer were cleaned prior to deposition. The procedure as follows

1. Clean in acetone for 5 min.
2. Wash in deionized water for 30 sec.
3. Heat (80 ℃) in 10 % HCl for 10 min.
4. Wash indeionized water for 30 sec.
5. Etch in dilyte hydrofluoric acid (5 % vol.HF) for 1 min.
6. Wash in deionized water.
7. Air blow-dry immediately.

3.5.2 Schottky-Barrier and Ohmic Contacts

The Schottky-barrier contact was generated between copper and n-type silicon wafer, while the ohmic contact was made between the aluminum and the back side of the silicon wafer. The evaporation was done in a high vacuum system. The evaperation pressure was 2*10E-5 Torr. The deposition thickness was monitored by a crystal thickness monitor (Fig. 3.6). The rates were kept constant at 2 Å/sec for Cu deposition and 4 Å/sec for Al. When each deposition was completed, the samples were cooled down to room temperature in the vacuum chamber to prevent oxidation.

The thickness of Cu thin film at the point where the

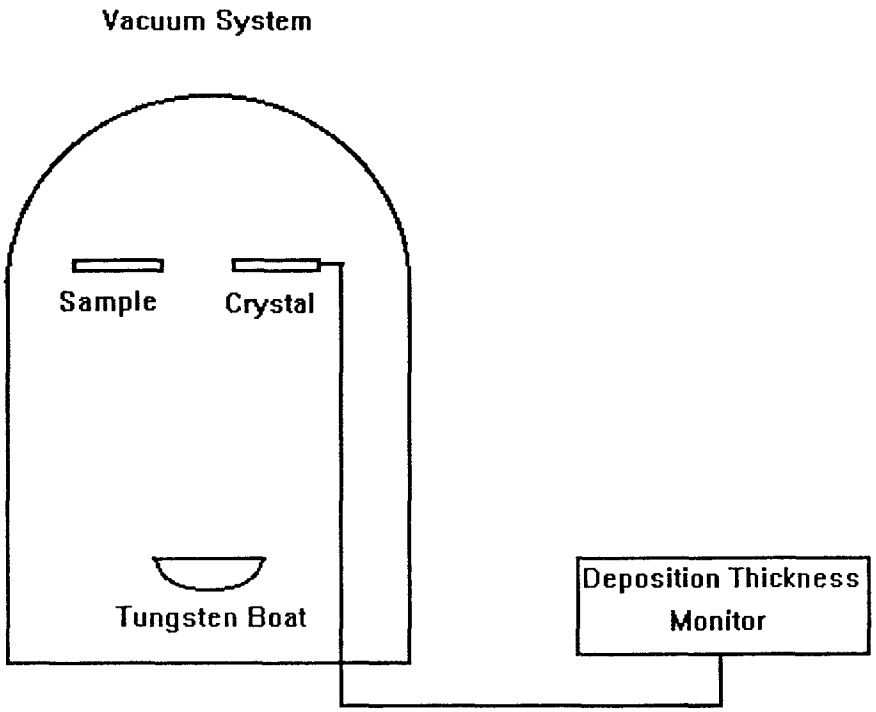

Fig. 3.6 The scheme of in-situ film deposition thickness monitoring

solar cell was formed, was only 100 Å. The reason for making such a thin film is to allow as much light as possible through the metal film, while keeping the electrical barrier. The thickness of the connecting wire was thicker, about 4000 Å, to reduce series resistance. The Al ohmic contact was also about 4000 Å for the same reason. After Al was deposited on Si substrate, the samples were transferred to another vacuum system for annealin, where they were heated up to 375 °C for 10 min. Then the wafers were cooled down to room temperature in the vacuum chamber to prevent oxidation.

The schemetic of a Schottky-barrier solar cell is shown in Fig. 3.7. The shaded areas are cells. The connections to the measuring point in the center are 6 mm long. One cell is textured and one cell is flat surface.

3.6 Schottky-Barrier Height Measurement

Schottky-barrier height of the solar cell was measured by the current-voltage method. Copper was deposited on a flat surface and a grooved surface of Si substrate to form two small areas (1 mm in diameter), respectively. The back of the silicon was deposited with Al to form ohmic contact as before. The samples were measured by Keithly.

3.7 Solar Cell's Characteristics Measurement

The schemetic of the setup to measure solar cells' short-circuit current and open-circuit voltage is shown in Fig.

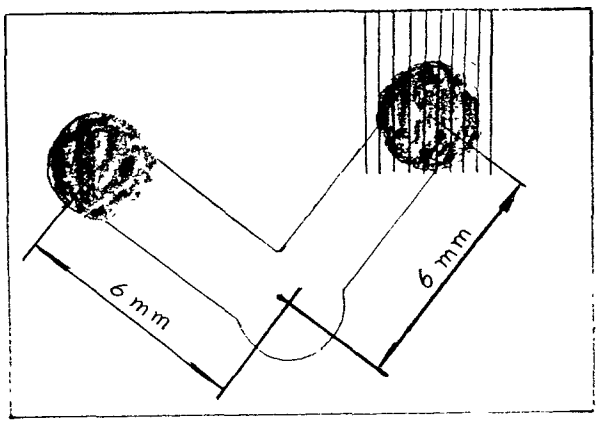

Fig. 3.7 Schematic of Cu/n-type Si Schottky-barrier solar cell. The shaded areas are semi-transparent Cu film.

3.8. By tilting the prism, the incident angle of the laser beam impinging on the surface of the solar cells is changed. For every change of incident angle, the data of short-circuit current and open-circuit voltage was recorded.

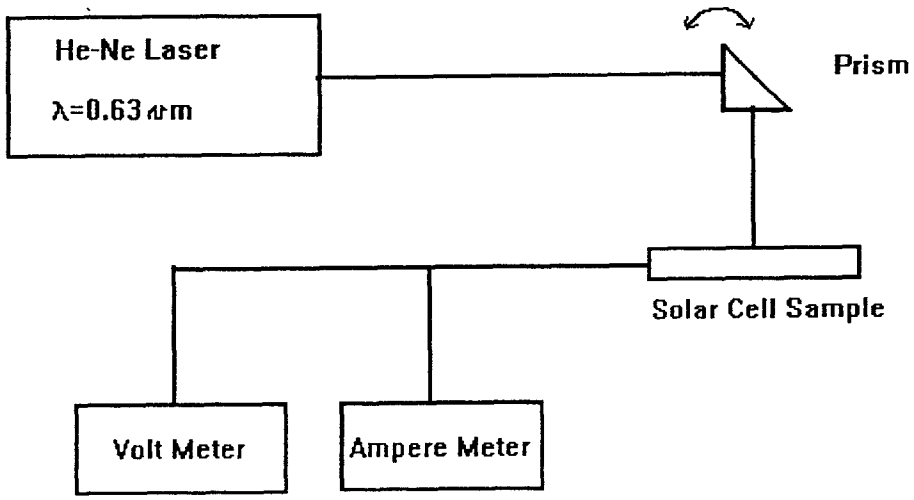

Fig. 3.8 The arrangement of shorh-circuit current and open-circuit voltage measurement

CHAPTER 4

EXPERIMENTAL RESULTS

4.1 The Surface Configuration Profile

The surface configurations were fabricated with the system introduced in section 3.1. The pattern profiles were measured by the various methods. Fig. 4.1 - 4.4 show optical micrographs of four different types of surface configuration profiles.

In Fig. 4.1, we present a profile of a V-shaped grooves created by laser etching in air. This result was achieved by using 20 pulses per groove, 0.03 mJ/cm of laser power. The line width is about 15 um and its depth 10 um, thus the angle is 74 degree. Fig. 4.2 shows the profile of an asymmetric V-shaped grooves which is fabricated under the same condition as the one shown in Fig. 4.1, except that we tilted the mirror by 15 degree (see Fig. 3.2).

M-shaped grooves were created by cotrolling the pulse number of the laser beam irradiated on silicon surface. For instance, in Fig. 4.3, the deep grooves were ablated by 20 pulses of the laser beam, while 10 pulses were used for the shallow ones. The depth of the shallow grooves were 5 um, as can be seen from the figure. The asymmetric M-shaped grooves were created the same as we did on asymmetric V-grooves by tilting the mirror 15 degrees. The profile is shown in Fig. 4.4. All patterns have a periodicity of 30 um.

Fig. 4.5 shows the profile of another V-shaped grooves measured by alpha-step recorder. The profile in the figure is upside down. The top in the figure is actually the bottom of the workpiece profile. Since the probe of the recorder is too thick to detect the details of the grooves, the bottom of the grooves seem rough.

Scanning electron micrograph of a V-shaped grooves is shown in Fig. 4.6. The distance between two grooves is 50 um, and the groove width 20 um. The grooves were fabricated by 15 pulses at total energy of 0.03 mJ/cm^2 . Melting occurs during laser ablation as shown in the micrograph. The upper edges of the grooves are surrounded by refrozen material. Fig. 4.7 shows the result for the laser incident on the sample while submerged in 5 % KOH solution. Fig. 4.8 shows another sample created by laser ablation in 5 % HF solution. Here somewhat less material is removed. The much smoother surfaces of the grooves are achieved as compared to Fig. 4.6 indicating that less melting and refrozen of material accur. Under the same condition, the grooves created with HF solution, are slight wider and deeper than with KOH solution. This is consistent with the facts that HF is an isotropic atchant and has higher etching rate on Si than KOH.

4.2 Barrier Height Measurement

We measured Schottky-barrier height of Cu/n-type Si contact on both flat and grooved surfaces. For flat surface, the

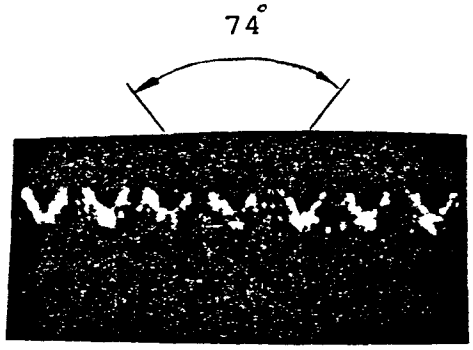

Fig. 4.1 Optical micrograph of V-shaped groove profile fabricated by laser ablation in air.

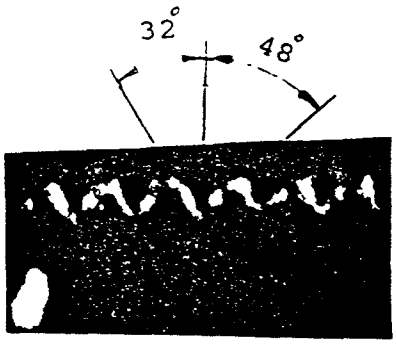

Fig. 4.2 Optical micrograph of asymmetric V-shaped groove profile fabricated by laser ablation in air.

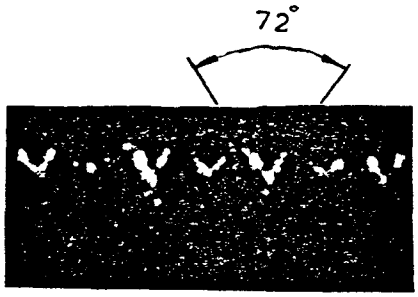

Fig. 4.3 Optical micrograph of M-shaped groove profile fabricated by laser ablation in air.

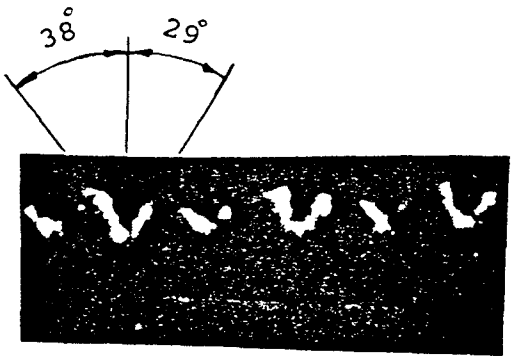

Fig. 4.4 Optical micrograph of asymmetric M-shaped groove profile fabricated by laser ablation in air

saturation current I_S is 8*10E-9 A for 1 mm diameter area; for grooved surface, I_S is 4*10E-8 A for the same area. By using Eq. (2.13), ϕ_{Bn} = 0.77 V for the flat surface contact and ϕ_{Bn} = 0.73 V for the grooved surface contact. The reason for the difference in the barrier height is possibly due to the barrier height lowering effect [1]. The I-V characteristics are shown in Fig. 4.9 flat surface contact and Fig. 4.10 for grooved surface contact, respectively.

4.3 Short-Circuit Current and Open-Circuit Voltage Measurement

The short-circuit current and open circuit voltage were measured by the system shown in Fig. 3.8. Fig. 4.11 - 4.18 show the curves of short-circuit current as a function of light incident angle for solar cells with flat surface and various textured surface configurations. For flat cell, change of light incident angle has very little or no effect on the short-circuit current; it does affect though the short-circuit current for patterned cells. It is worth to point out that incident light impinging in an angle has a different spot size, though the total optical power should remain the same. Case should be taken thus, to include all light activating the solar cell. The curves for flat cells in Fig. 4.11 - 4.18 confirms this point.

Fig. 4.19 - 4.26 show the improvement in short-circuit current of Schottky-barrier solar cells with different patterned surface over a flat surface cell as a function of

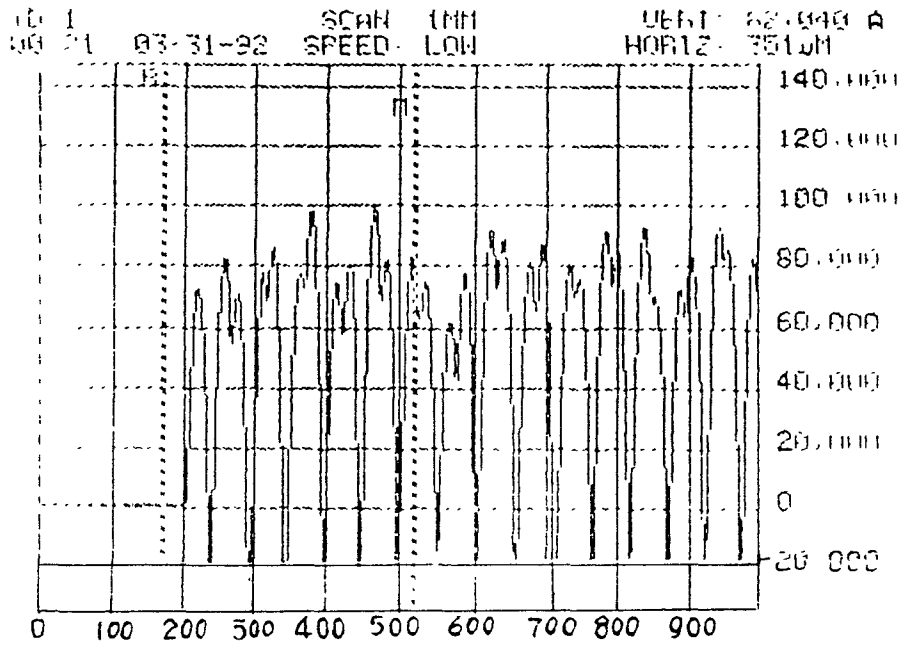

Fig. 4.5 V-shaped groove profile fabricated by laser ablation in air. The profile was measured by alpha-step recorder.

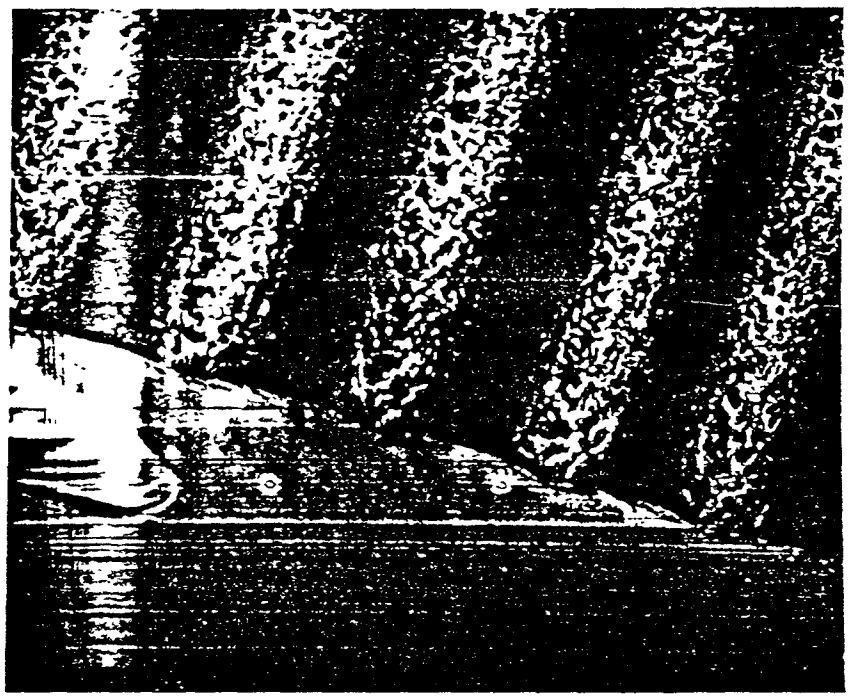

Fig. 4.6 Scanning electron micrograph of V-shaped grooves ablated with KrF UV laser in solution (5% vol.HF).

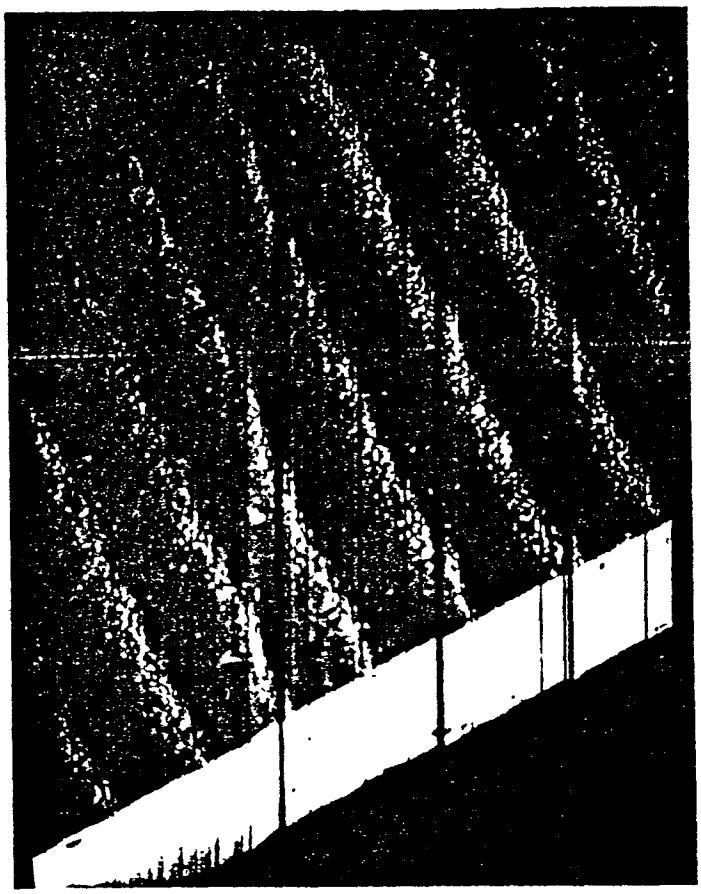

Fig. 4.7 Scanning electron micrograph of V-shaped grooves ablated with KrF UV laser in solution (5% wt.KOH).

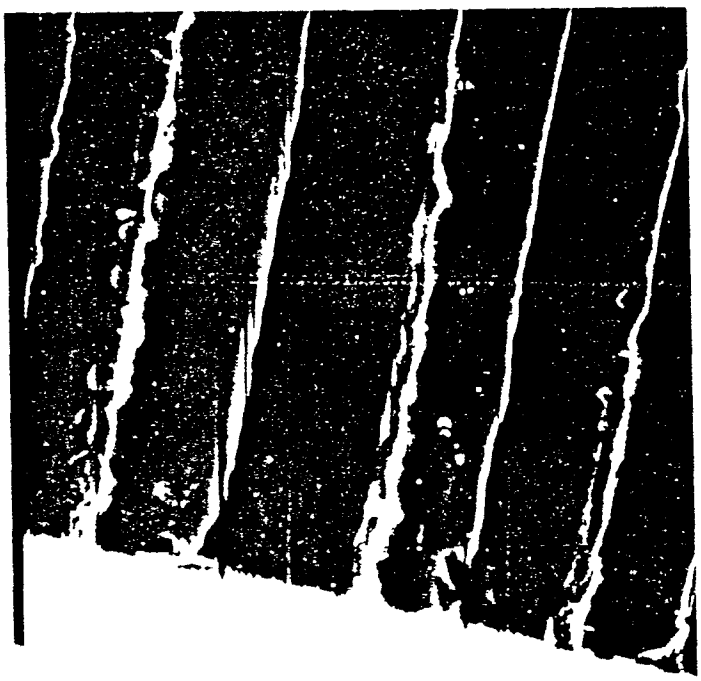

Fig. 4.8 Scanning electron micrograph of V-shaped grooves fabricated by laser ablation in air.

saturation current I is $8*10^{-9}$ A for 1 mm diameter area; for grooved surface, I is $4*10^{-8}$ A for the same area. By using Eq. (2.13), ϕ_{Bn} = 0.77 V for the flat surface contact; ϕ_{Bn} = 0.73 V for the grooved surface contact. The reason for the difference of the barrier height is due to the barrier height lowering. The I-V characteristics are shown in Fig. 4.9 flat surface contact and Fig. 4.10 for grooved surface contact, respectively.

4.3 Short-Circuit Current and Open-Circuit Voltage Measurement

The short-circuit current and open circuit voltage was measured by the system shown in Fig. 3.8. Fig. 4.11 - 4.18 show the curves of short-circuit current as a function of light incident angle for solar cells with flat surface and various textured surface configurations. For flat cell, change of light incident angle has very little or no effect on short-circuit current; it does affect though short-circuit current for patterned cells. It is worth to point out that incident light impinging in an angle has a different spot size, though the total optical power should remain the same. A case should be thus taken to include all light in the activation of the solar cell. The curves for flat cells in Fig. 4.11 - 4.18 prove this point.

Fig. 4.19 - 4.26 show the improvement in short-circuit current of Schottky-barrier solar cells with different patterned surface over a flat surface cell as a function of

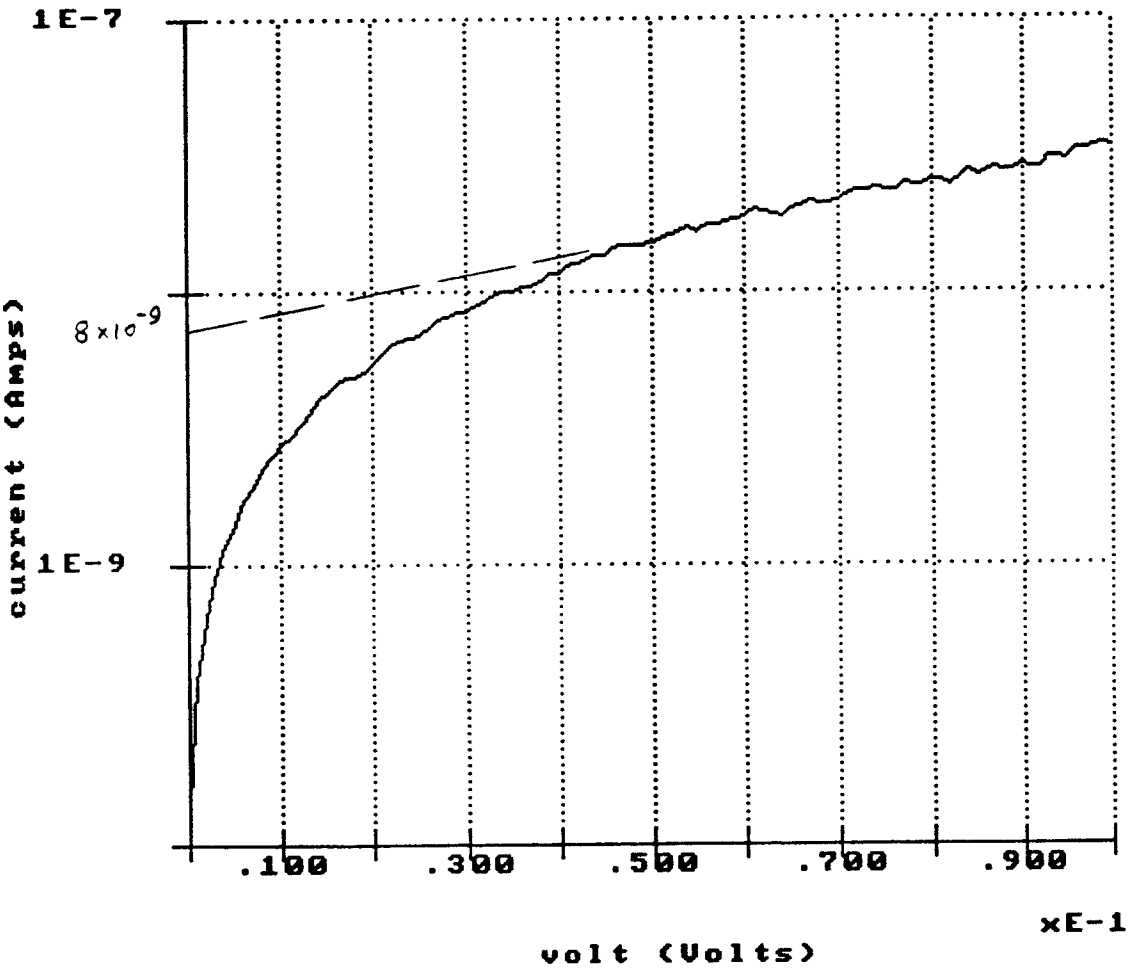

Fig. 4.9 Log(I) versus V for a Cu/n-type Si Schottky-barrier diode. The contact is on a flat surface.

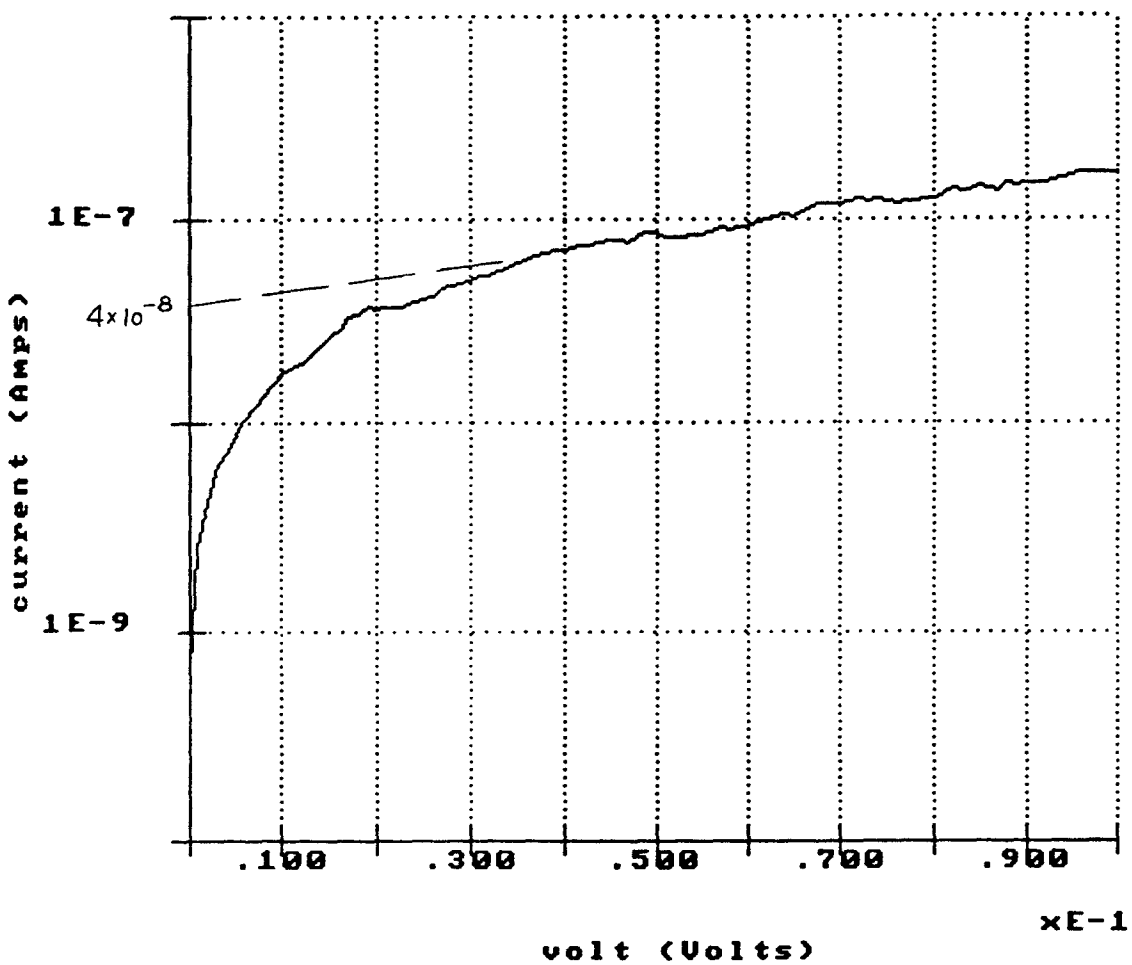

Fig. 4.10 Log(I) versus V for a Cu/n-type Si Schottky-barrier diode. The contact is on a grooved surface.

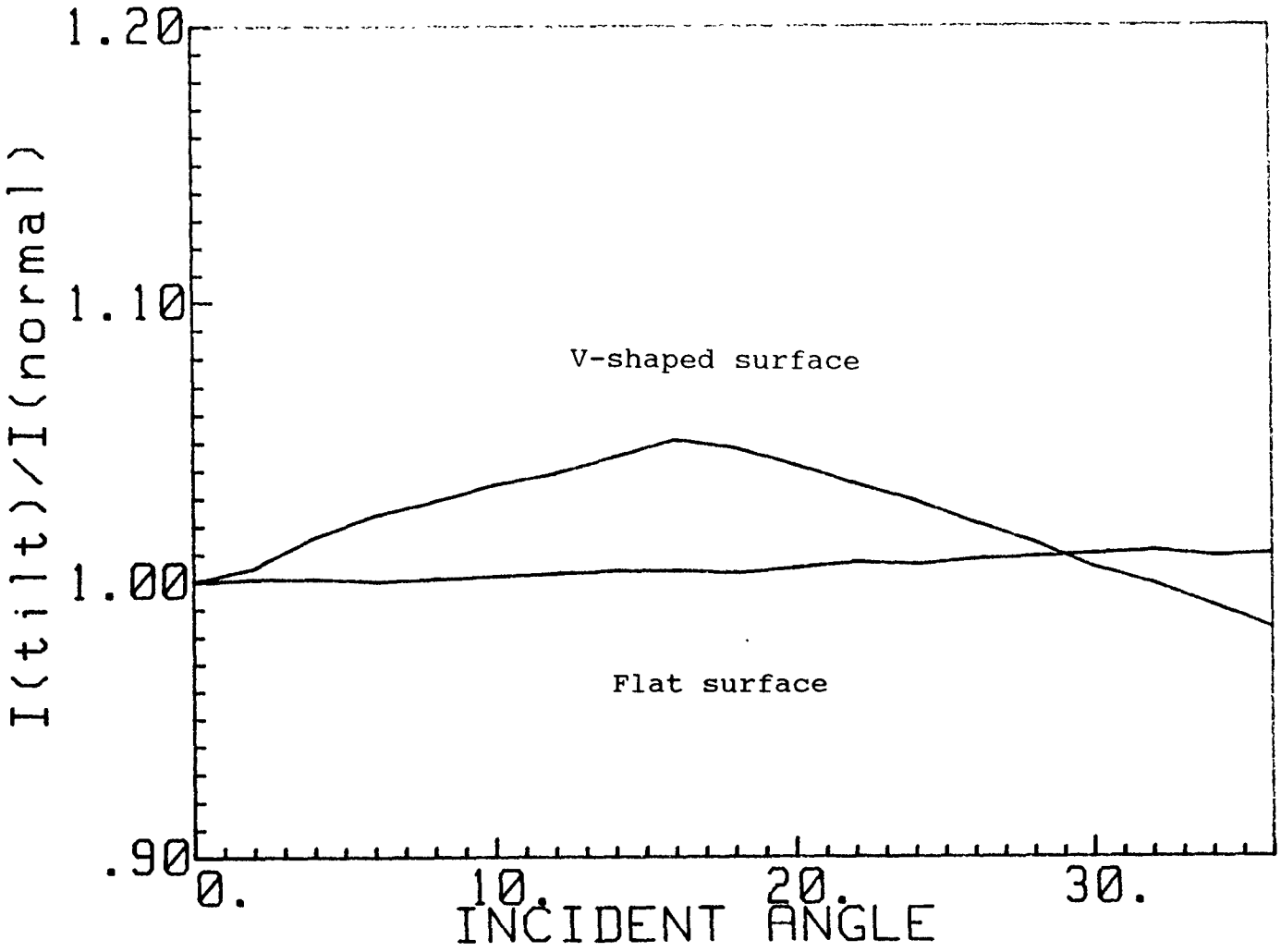

Fig. 4.11 Short-circuit current as the function of inciden angle for Schottky-barrier solar cells with flat surface and V-shaped groove surface created by laser ablation in solution (5% wt KOH).

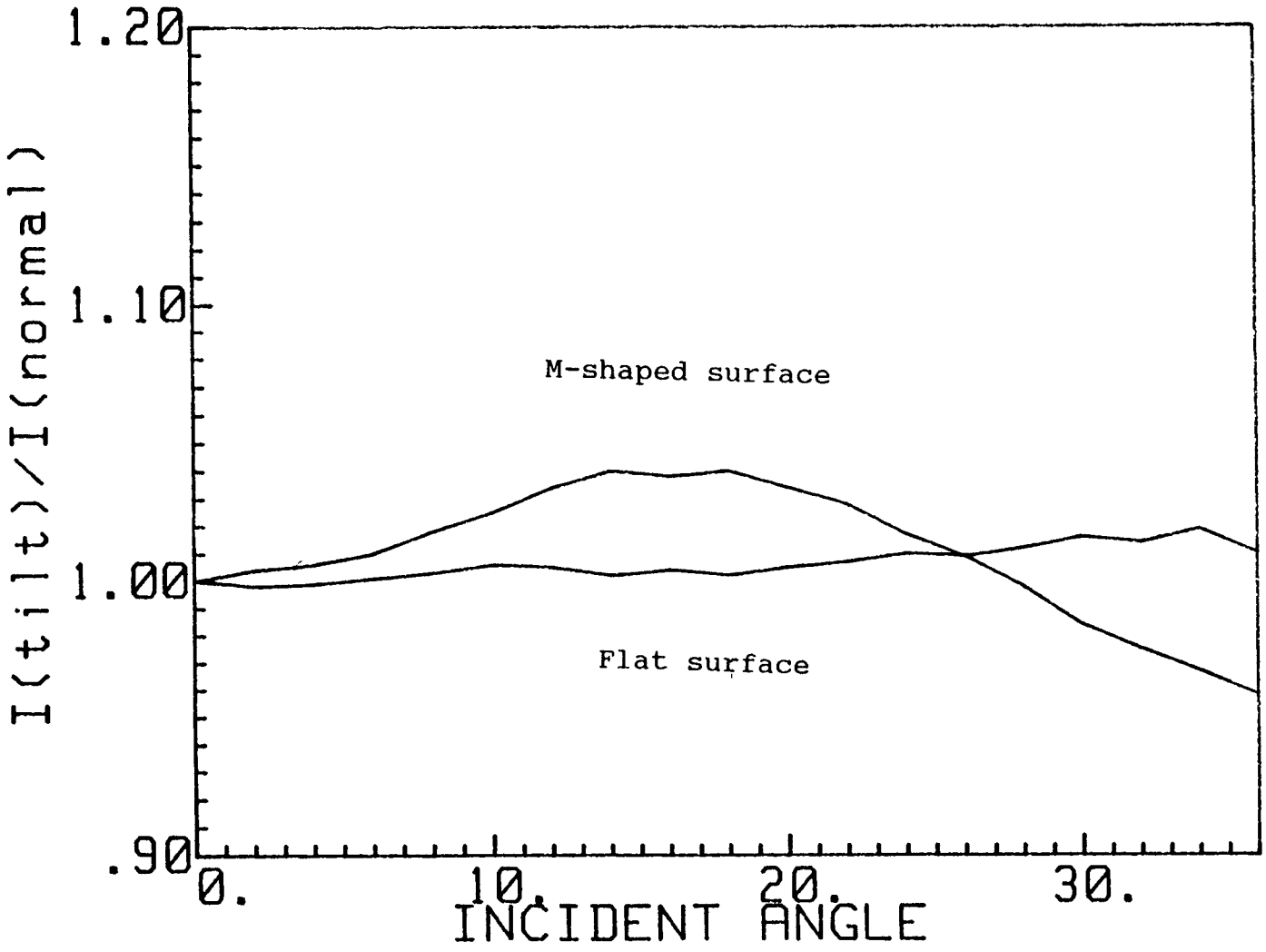

Fig. 4.12 Schort-circuit current as the function of incident angle for Schottky-barrier solar cells with flat surface and M-shaped groove surface created by laser ablation in solution (5% wt KOH).

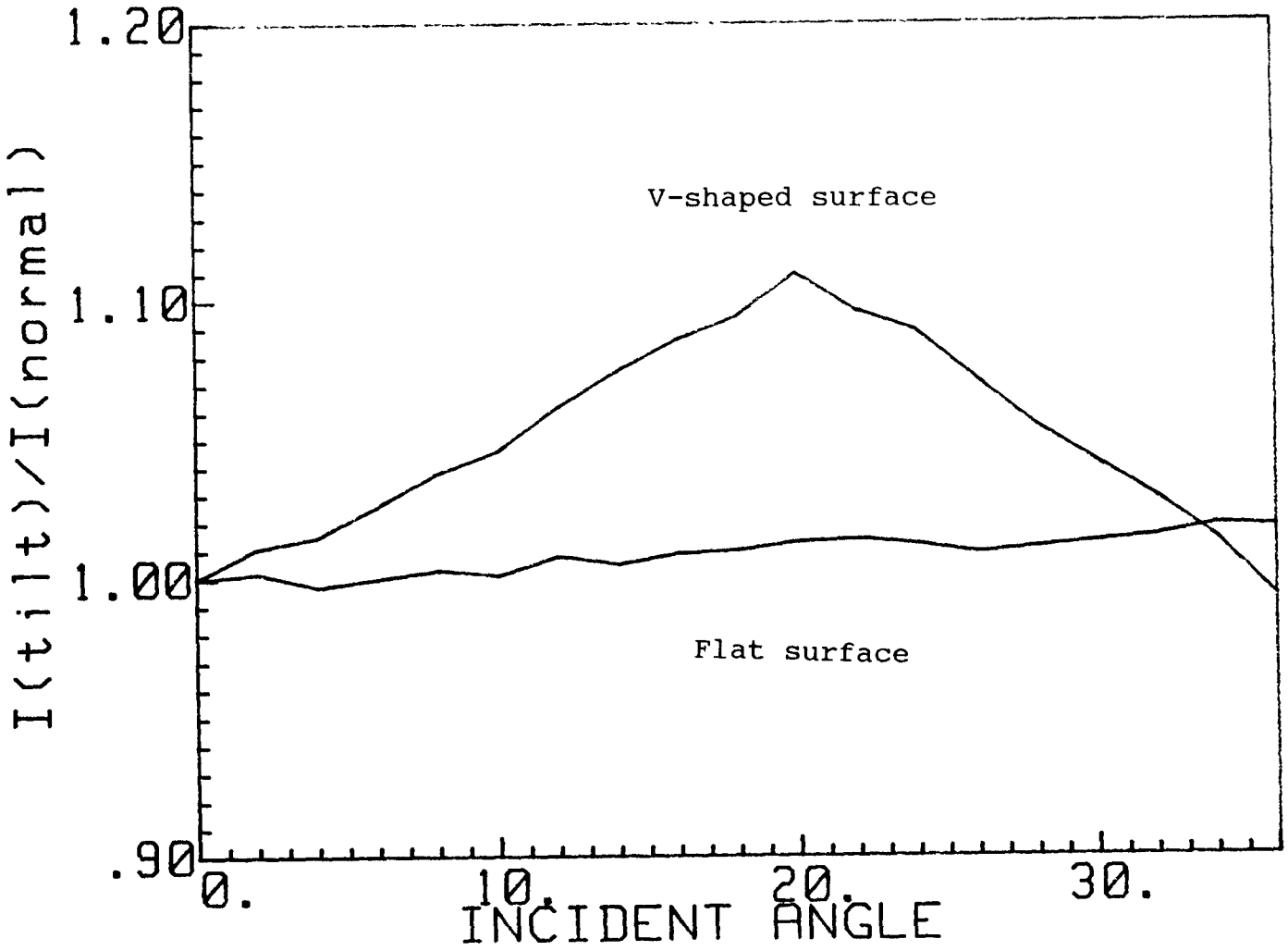

Fig. 4.13 Short-circuit current as the function of inciden angle for Schottky-barrier solar cells with flat surface and V-shaped groove surface created by laser ablation (5% vol HF).

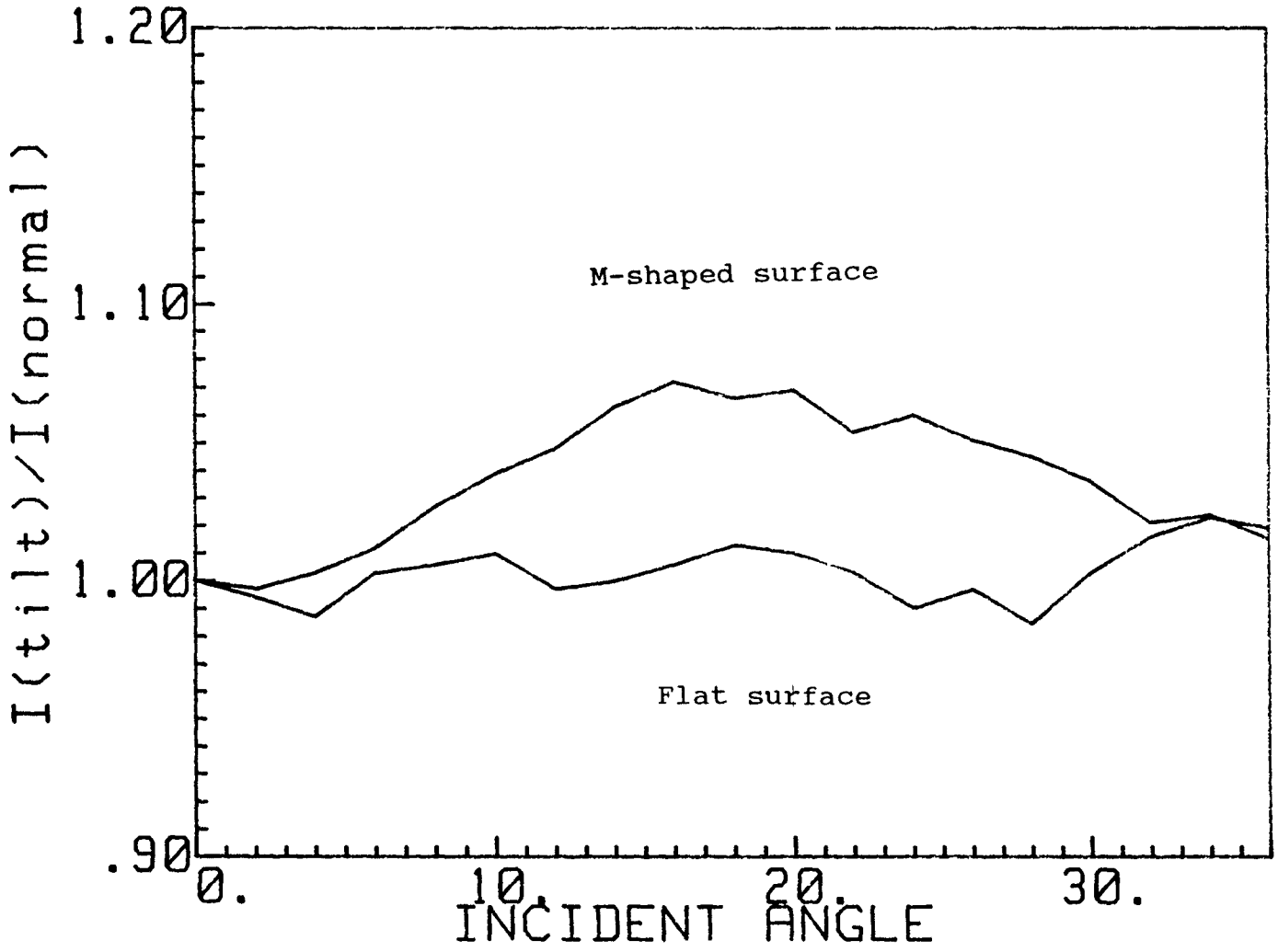

Fig. 4.14 Short-circuit current as the function of incident angle for Schottky-barrier solar cells with flat surface and M-shaped groove surface created by laser ablation (5% vol HF)

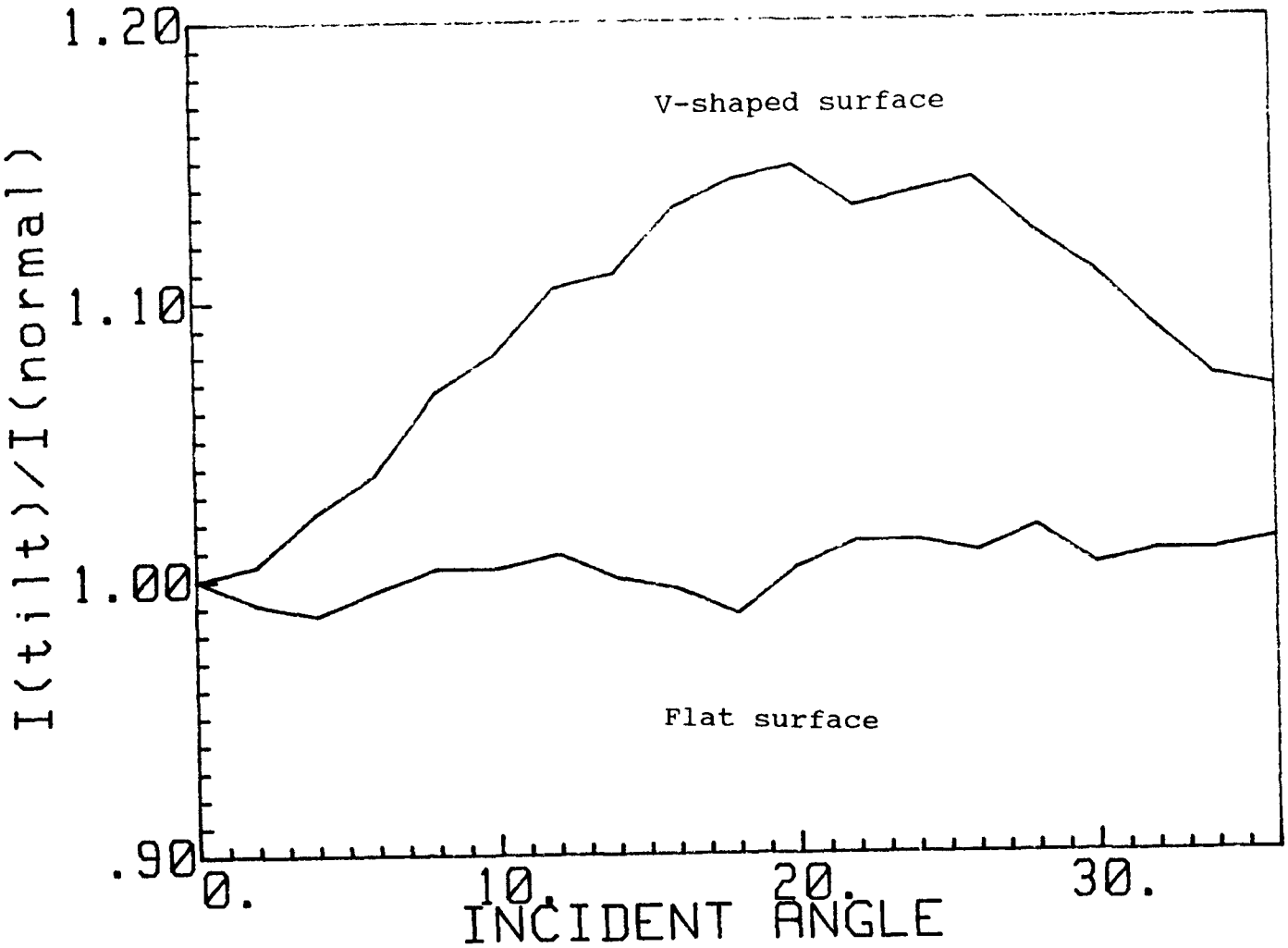

Fig. 4.15 Short-circuit current as the function of incident angle for Schottky-barrier solar cells with flat surface and V-shaped groove surface created by laser ablation in air.

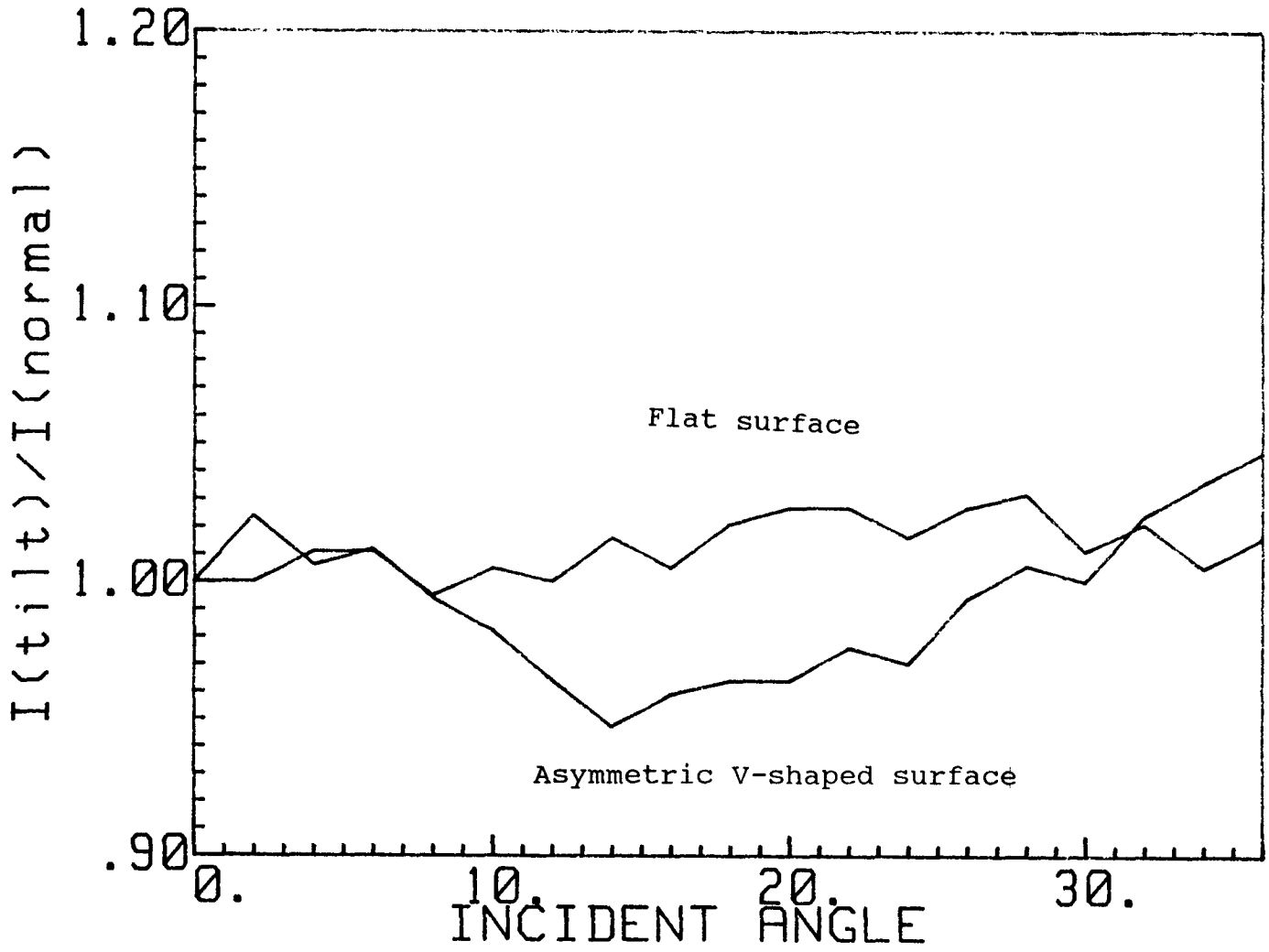

Fig. 4.16 Short-circuit current as the function of incident angle for Schottky-barrier solar cells with flat surface and asymmetric V-shaped groove surface created by laser ablation in air.

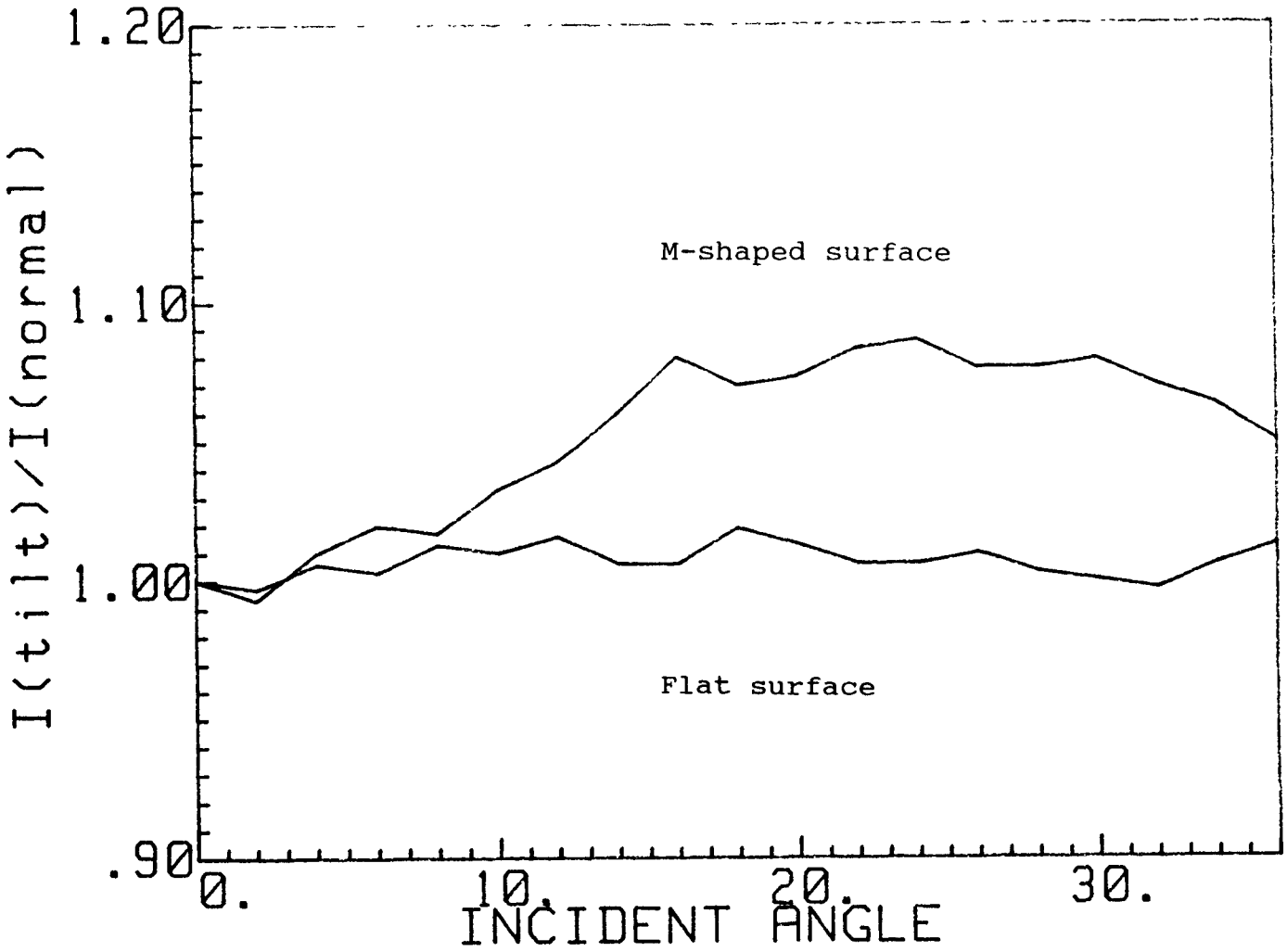

Fig. 4.17 Short-circuit current as the function of incident angle for Schottky-barrier solar cells with flat surface and M-shaped groove surface created by laser ablation in air.

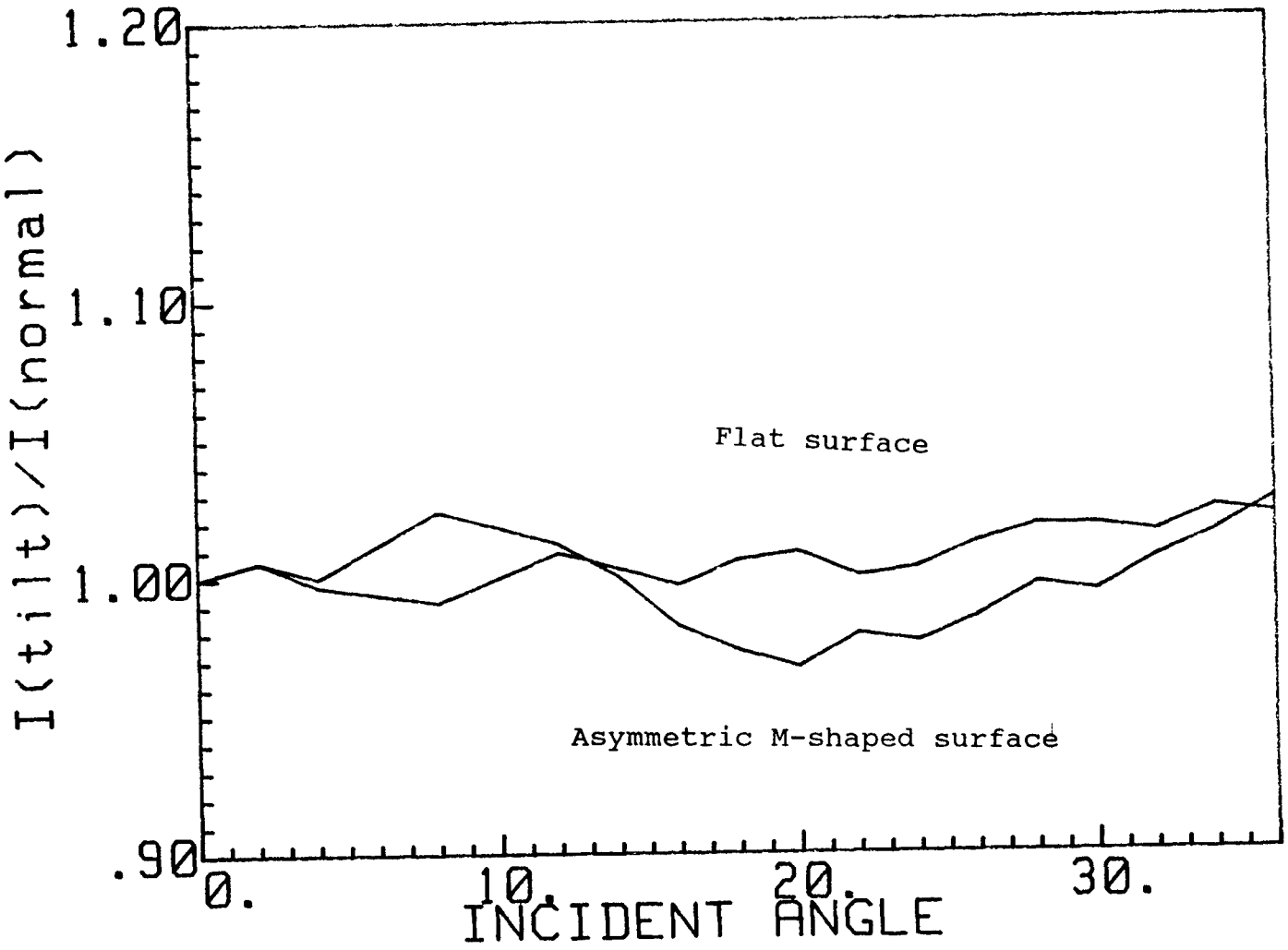

Fig. 4.18 Short-circuit current as the function of incident angle for Schottky-barrier solar cells with flat surface and asymmetric M-shaped groove surface created by laser ablation in air.

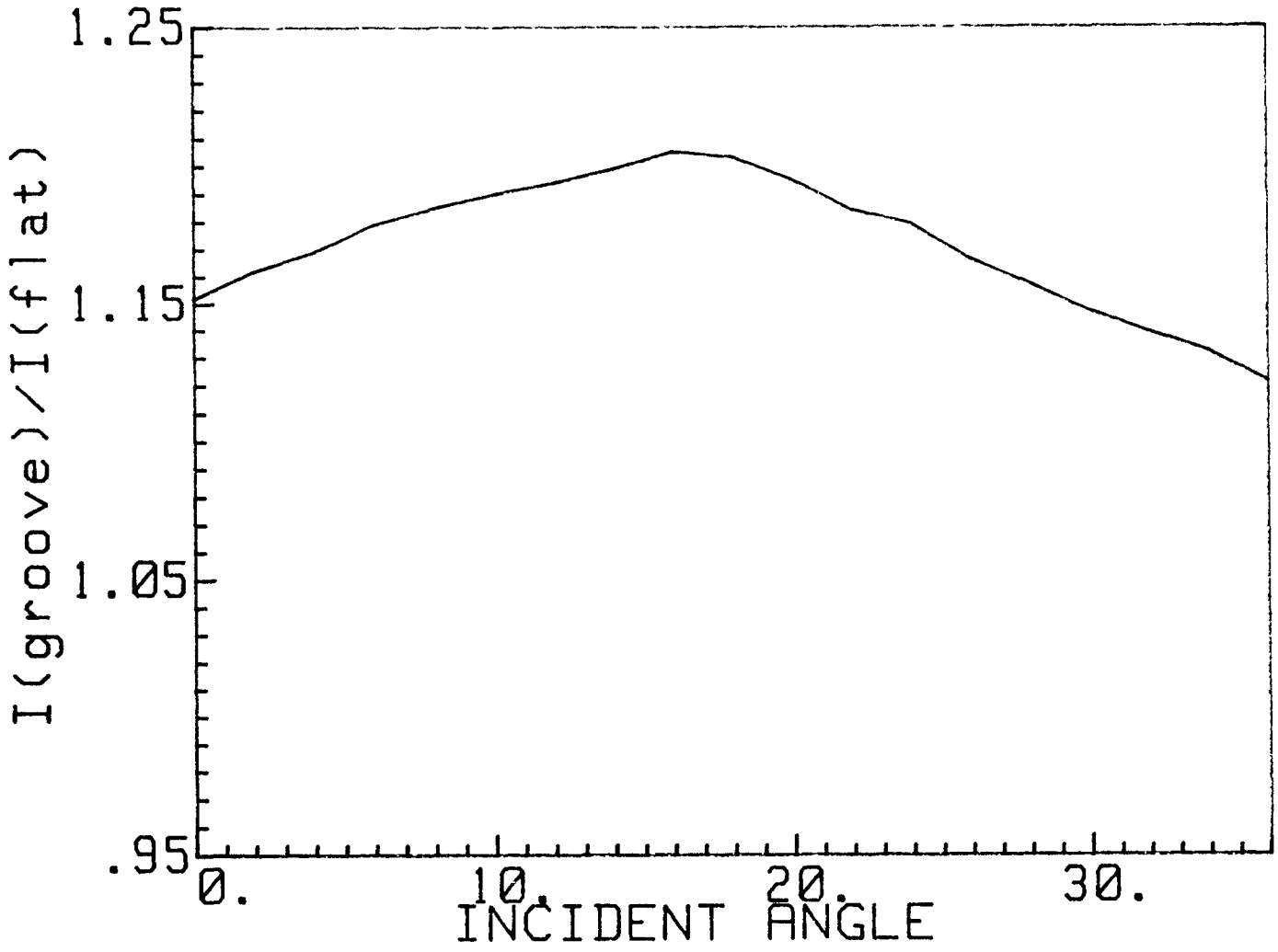

Fig. 4.19 Improvement in short-circuit current of Schottky-barrier solar cell for textured surface over flat surface. The textured surface is V-shaped grooves created by laser ablation (5% wt KOH).

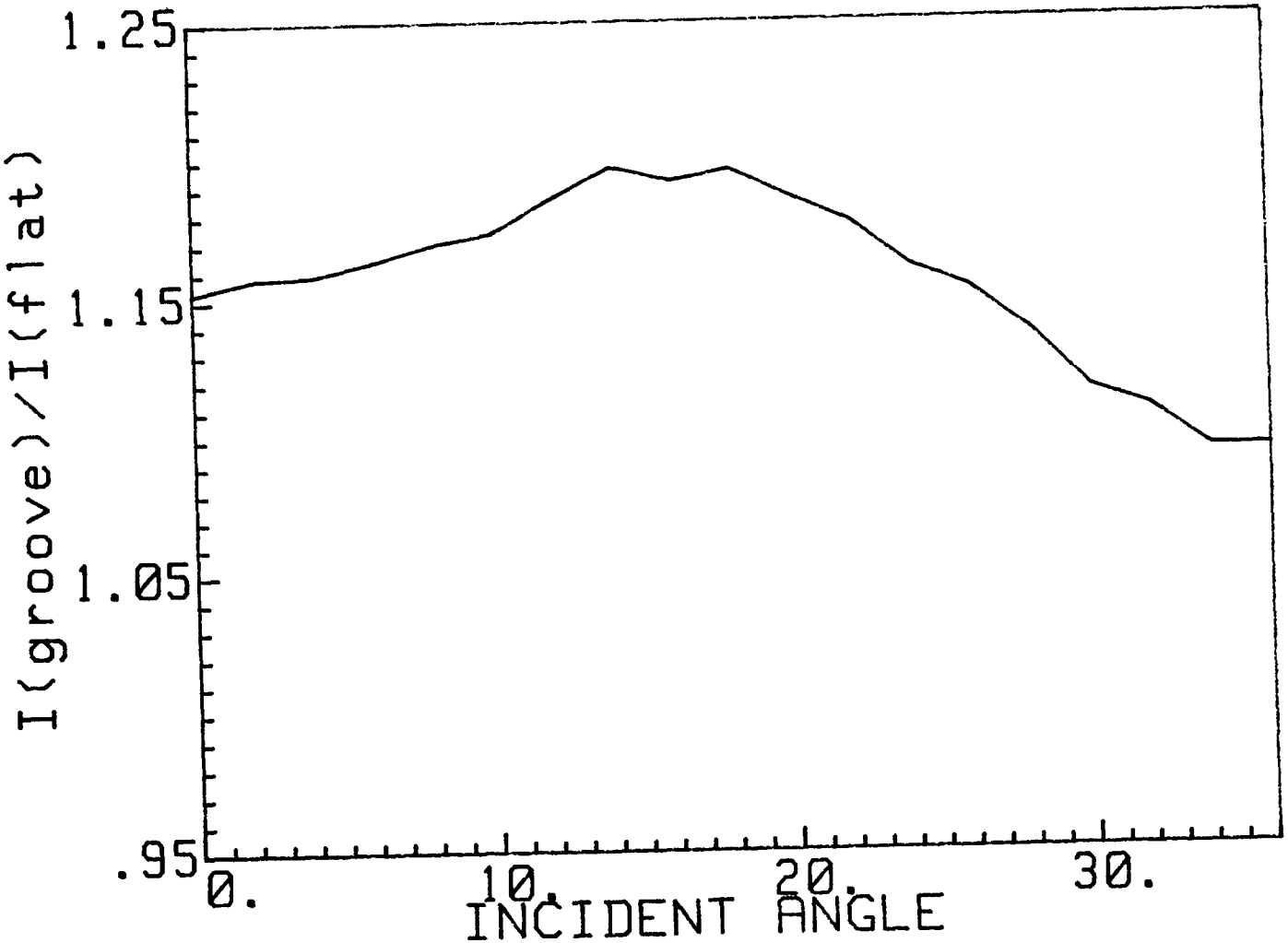

Fig. 4.20 Improvement in short-circuit current of Schottky-barrier solar cell for textured surface over flat surface. The textured surface is M-shaped grooves created by laser ablation in solution (5% wt KOH).

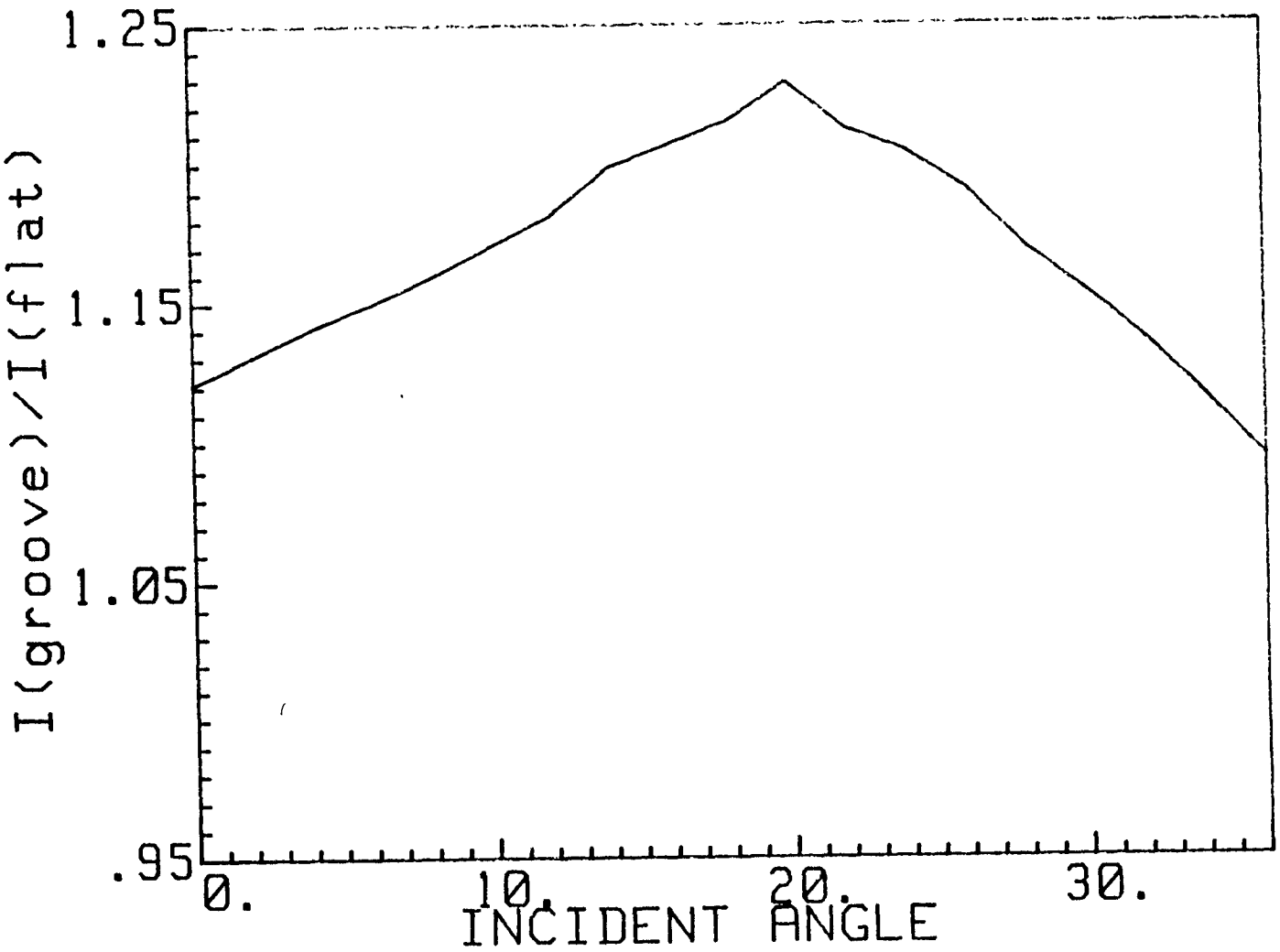

Fig. 4.21 Improvement in short-circuit current of Schottky-barrier solar cell for textured surface over flat surface. The textured surface is V-shaped grooves created by laser ablation (5% vol HF).

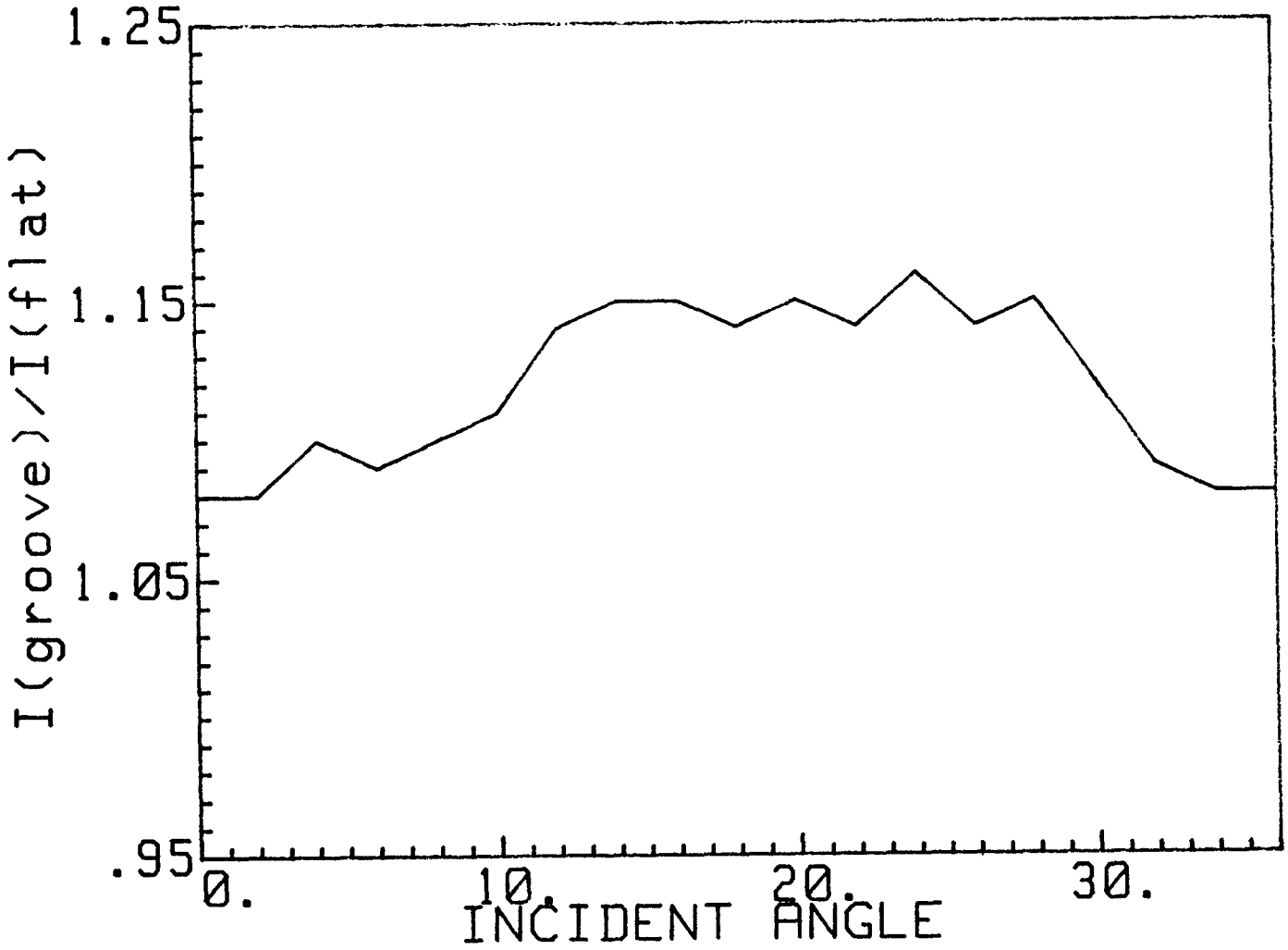

Fig. 4.22 Improvement in short-circuit current of Schottky-barrier solar cell for textured surface over flat surface. The textured surface is M-shaped grooves created by laser ablation in solution (5% vol HF).

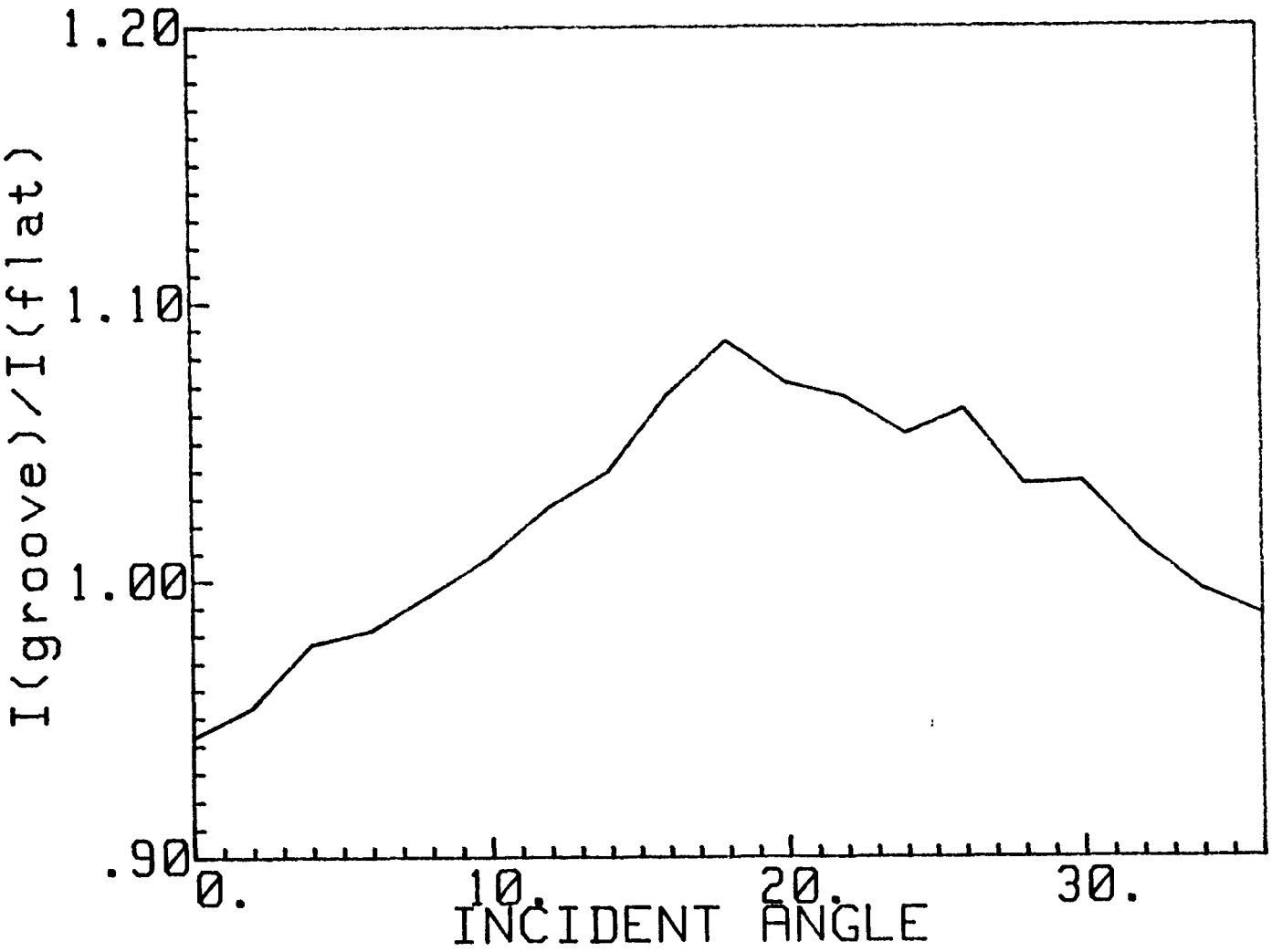

Fig. 4.23 Improvement in short-circuit current of Schottky-barrier solar cell for textured surface over flat surface. The textured surface is V-shaped grooves created by laser ablation in air.

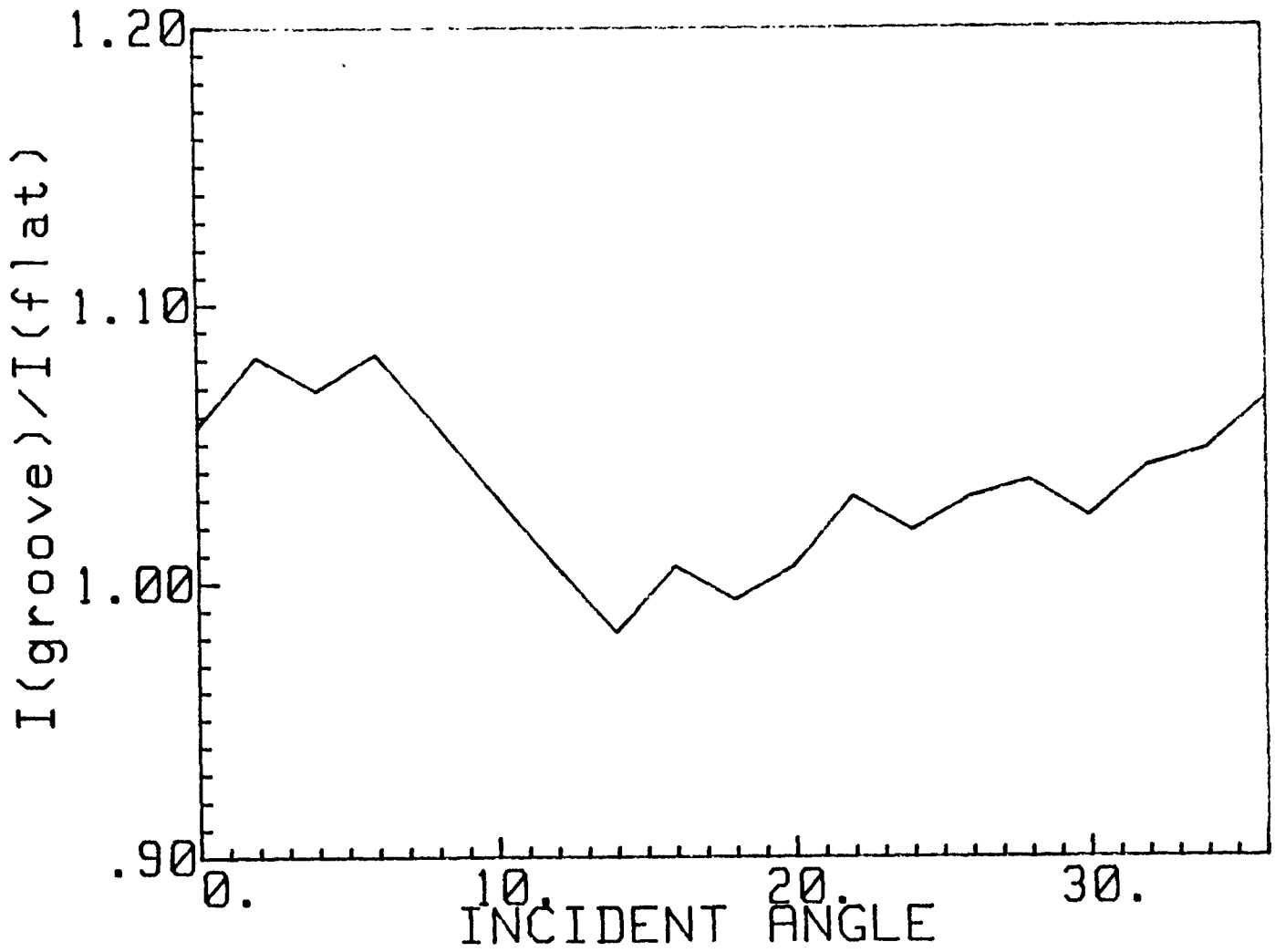

Fig. 4.24 Improvement in short-circuit current of Schottky-barrier solar cell for textured surface over flat surface. The textured surface is asymmetric V-shaped grooves created by laser ablation in air.

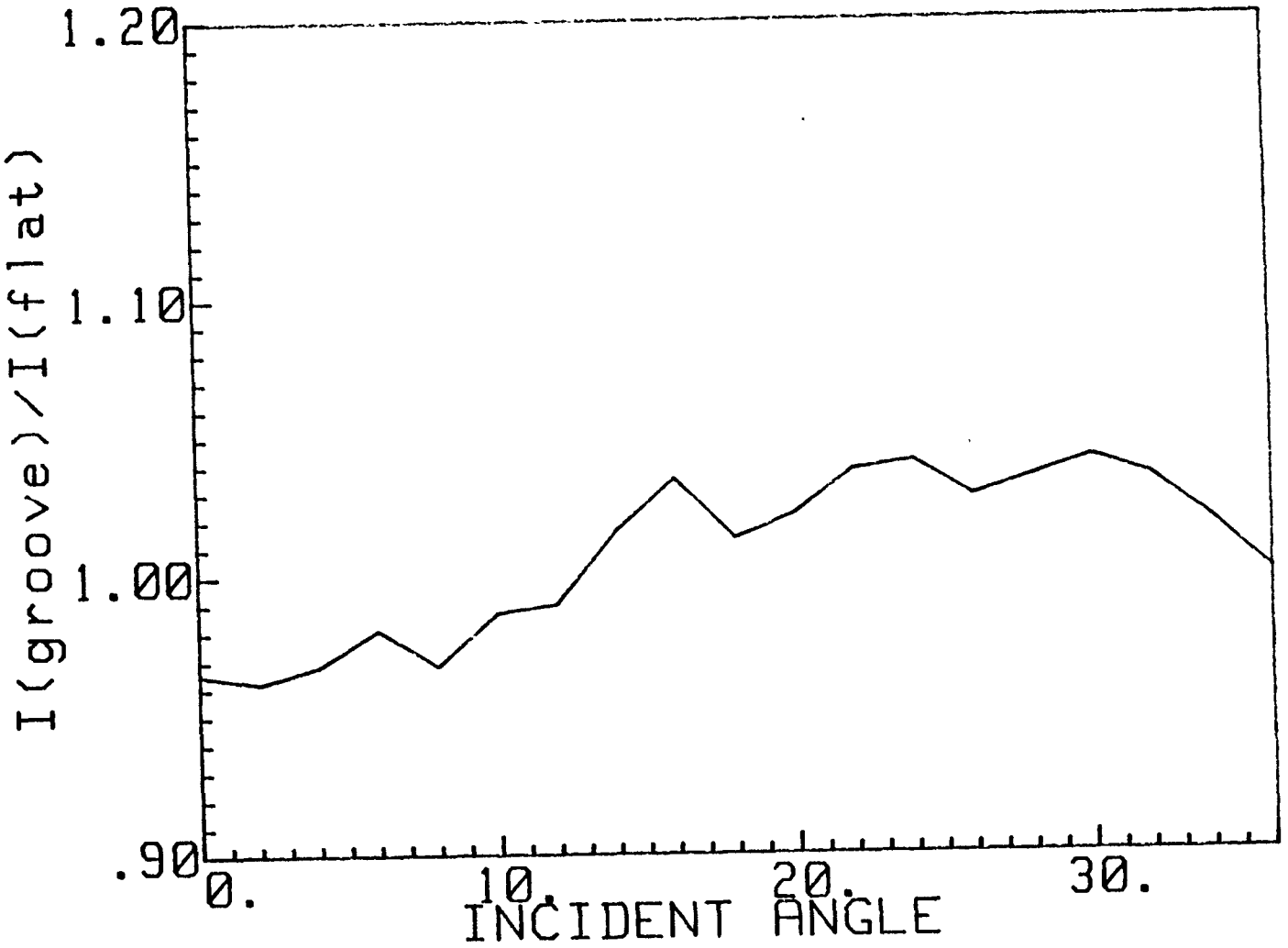

Fig. 4.25 Improvement in short-circuit current of Schottky-barrier solar cell for textured surface over flat surface. The textured surface is M-shaped grooves created by laser ablation in air.

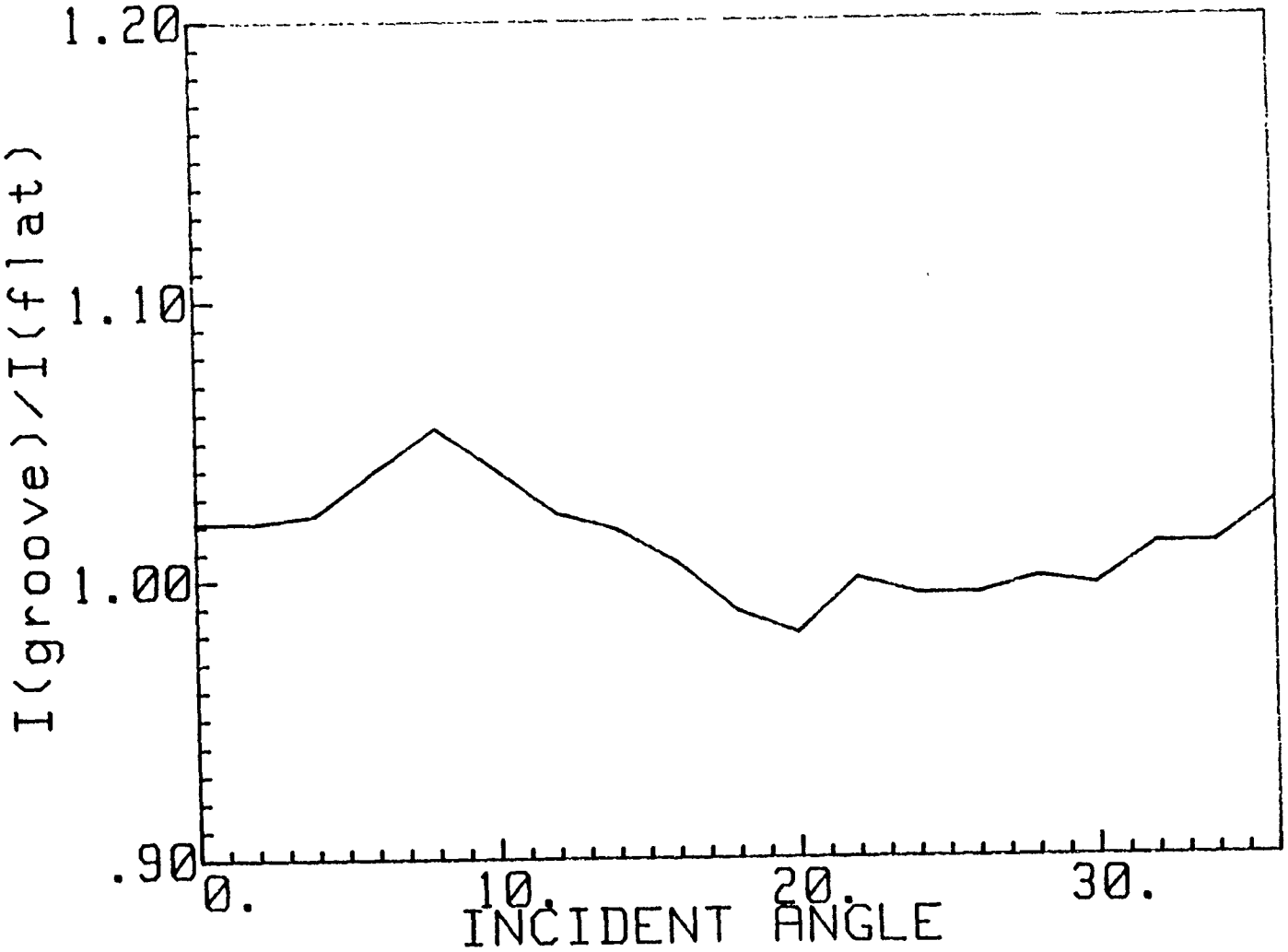

Fig. 4.26 Improvement in short-circuit current of Schottky-barrier solar cell for textured surface over flat surface. The textured surface is asymmetric M-shaped grooves created by laser ablation in air.

CHAPTER 5

DISCUSSION

In this thesis we aimed to prove that textured solar cells are more efficient than flat solar cells by absorbing more light via multiple reflection in the textured surface. This is suggested by comparing the short-circuit current for both cells. The improvement not only depends on the surface configuration, but also on the methods of fabrication.

For the surface patterns created by laser ablation in solutions, both V-shaped and M-shaped grooved surface configurations showed similar improvement in short-circuit current over a flat surface device. The short-circuit current varies as a function of the light angle of incidence and peaks around 20 degrees. This further proves to our opinion, that improvement in the cell design is mainly due to an increase in the number of ray reflections within the grooves. For the surface configurations created by laser ablation in air, the overall performence is not as good as those solar cells with the same patterns created in solutions. This indicates the damaging effect of a too strong ablation process.

The peak short-circuit current, for V-shaped and M-shaped grooves, appears at about 20 degrees of incident light angle. The peak short-circuit current, for asymmetric V-shaped and M-shaped patterns, appears at normal light incident angle. This suggests that a solar cell with an

appropriately designed asymmetric V-shaped or M-shaped configurations may deliver maximum power when light is normally incident on the surface of the solar cell. The experimental results were comparable as far as the efficiencies of these two cells.

Most of the improvement of light collection efficiency is due to the increase in short-circuit current. No practical improvement is detected in the open-circuit voltage, which means that the Schottky-barriers have little difference for textured and non-textured surfaces. This is because of the subsequent increase in the saturation current as the effective surface area is increased.

Due to its low open-circuit voltage, Schottky-barrier solar cells with efficiency of more than 15% have not been reported. The high saturation current, Is, limits the free flow of photo-generated current. To reduce Is, usually a thin insulating oxide film is used between the metal and the semiconductor. The interfacial layer of oxide can increase the open-circuit voltage. In our case, we have achieved efficiencies of about 5%; yet it should be mentioned that the measurements have been taken with a red light source. In general, this method may be useful to other types of solar cells as well, such as, p-n junctions.

The Schottky-barrier heights of Cu/n-type Si interface are different for flat and patterned surfaces. The reason is due to the Schottky-barrier lowering potential. Since surface patterning changes the geometrical surface

configurations, the field intensity may change as well [15]. The higher field intensity on patterned interface leads to a larger Schottky barrier lowering potential, thus the barrier height on patterned interface may differ from flat interface. In our case a lower barrier of 30 mV has been measured when comparing grooved and non-grooved barriers.

CHAPTER 6

CONCLUSION

Improvement of 5% to 20% in light collection efficiency were shown for different patterned surface solar cells over flat cells. Different geometric configurations have been created by means of laser abltation in air and solutions. Cu/n-type Si Schottky-barier solar cells have been made on different patterned substrates. Short-circuit current and open-circuit voltage have been measured for these cells. Symmetric V-grooves and symmetric M-shape grooves were founde the best patterns at 20 incident light.

Laser ablation in solutions in a simple thin-film cell arrangement, has been found a better way to create smooth, damage-free grooves than that of laser direct writing method, even though the latter technique provides a more effective way to create grooves.

BIBLIOGRAPHY

1. Sze, S. M., "Physics of Semiconductor Devices." 2nd.Ed. New York, John Wiley & Sons,Inc., (1981): 247-307.

2. Hamakawa, Y. "Phopovoltaic Power." Scientific American, 256 (1987): 86-87.

3. Fischetti, M.A., "Photovoltaic-cell Technologies Joust for Position." IEEE Spectrum, 21 (1984): 40-43

4. Sze, S.M."Semiconductor Devices Physics and Technology." New York, John Wiley & Sons, Inc. (1985): 287-300, 451-456.

5. Streetman, B.G., "Solid State Electronic Devices." 2nd. Ed., New Jersey, Prentics-Hall, Inc., (1980): 210-218.

6. Arndt, R.A., "Optical Properties of the COMSAT Non-Reflective Cell." The 11th IEEE Photovoltaic Specialists Conference." (1975): 40-43.

7. Menlenberg, A., "Radiation Damage to the COMSAT Non-Ref lective Cell." The 11th IEEE Photovotaic Specialists Conference, (1975): 204-208.

8. Baraona, C.R, "V-grooved Silicon Cells." The 11th IEEE Photovoltaic Specialists Conference, (1975): 44-48

9. Campbell, P., "Light Trapping Properties of Pyramidally Textured Surfaces." J.Appl.Phys. 62 (1987): 243-249

10. Allmem, Martin von, "Laser-Beam Interactions with Materials." Springer-verlag, Berlin, (1987): 6-46

11. Brown, W., "Laser and Electron Beam Solid Interactions and Material Processing." North Holland, (1981): 23-47.

12. Pulfrey, D.L., "Photovoltaic Power Generation." Van Nostrand Co. (1978): 12-31.

13. Boyd, I.W., "Surface Studies with Laser." Chem. Phys. 33 (1983): 193-195

14. Henry, C.H., "Limiting Efficiecies of Ideal Single and Multiple Energy Gap Terrestrial Solar Cells." J.Appl. Phys. 51 (1980): 2011-2013.

15. Von Gutfeld, R.J. and R.T. Hodgson, "Laser Enhanced Etching in KOH." Appl. Phys. Lett. 40 (1982): 353-356.

16. Moutonnet, D., in "Laser Processing and Diagnoserices." edited by D. Bauerle, New Yowk, Spring Verlag, (1984): 339-342.

17. Chappell, T.I. "The V-Grooved Multijunction Solar Cell." IEEE Trans. on Electron Devices, ED-26, No.9, (1979): 1365-1368.

18. McOuat, R., and D.L. Pulfrey, "Analysis of Silicon Schottky Barrier Solar Cells." The 11th IEEE Photovotaic Specialists Conference, (1975): 371-375.

19. Backus, C.E., "Solar Cells." New York, IEEE Press, Inc. (1976): 171-190.

20. Grebel, H., B.Iskandar, and K.G. Shappard,"Photoelectrochemical Etching of n-InP in a Thin-Film Cell." Appl. Phys. Lett. 25 (1989): 2655-2657.

21. Grebel, H., B. Iskandar, and K.G. Shappard, "The Effect on Nonlinear Ion Transport on the Rate of Laser-Induced Electrochemical Etching of Semiconductors", J. Appl. Phys. 67 (1990): 1947-1949.

22. Ellis, A.B., J.M. Bolts, and M.S. Wrighton, "Characterization of n-type Semiconductor Indium Phosphide Photoelectrodes." J. Electrochem. soc., 124 (1977): 1603-1605.

23. Manolis, Constantinos, "Schottky-Barrier Solar Cells; Surface Patterning for Efficient Light Collection." NJIT, (1989): 67-68.

24. Pulfrey, D.L., and R.F. McOuat, "Schottky-barrier Solar Cell Calculations." Appl. Phys. Lett. 24 (1974): 167-169.

25. Singh R.,and J. Shewchum, "Current Conduction in Schottky Barrier Solar Cells with an Interfacial Layer." Photovoltaics and Materials Conference, 6 (1976): 147-149.

26. McOuat, R.F., and D.L. Pulfrey, "A model for Schottky-barrier Solaer Cell Analysis." J. Appl.Phys. 47 (1976): 2113-2119.

27. Anderson, W., and R.A. Milano, "I-V Characteristics for Silicon Schottky Solar Cells." Proceedings of the IEEE, (1975): 206-208.

28. Klein, M., and T.E. Furtak, "Optics." 2nd Ed., New York, John Wiley & Sons, Inc. (1986): 89-112.

29. Morrison, S.R., "Electrochemistry at Semiconductor and Metal Electrodes." New York, Plenum Press, (1980): 157-164.

30. Ostermeyer, F.W.Jr., "Hole Transport Equation Analysis

of Photoelectrochemical Etching Resolution." J. Appl. Phys. 58 (1985): 4390-4392.

31. Braun, David M.,"Low Reflectivity Triangular Groove Surface Relief Gratings for InP/InGaAs/InP Photodetectors" Appl. Opt. 28 (1989): 4006-4009.